IEEE Access
Multidisciplinary ⋮ Rapid Review ⋮ Open Access Journal

Received June 22, 2021, accepted July 2, 2021, date of publication July 6, 2021, date of current version July 14, 2021.

Digital Object Identifier 10.1109/ACCESS.2021.3095116

On Novel Adaptive Coordinated Control for Spacecraft Formation: An Adjustable Performance Approach

DANGJUN ZHAO[1], KAI JIN[2], AND CAISHENG WEI[1]
[1]School of Aeronautics and Astronautics, Central South University, Changsha 410083, China
[2]The 54th Research Institute of CETC, Shijiazhuang, Hebei 050081, China

Corresponding author: Caisheng Wei (caisheng_wei@csu.edu.cn)

This work was supported by the Open Funds of National Key Laboratory of Aerospace Flight Dynamics and the Key Laboratory of Space Intelligent Control Technology, China, under Grant ZDSYS-2019-01.

ABSTRACT This paper investigates an adaptive coordinated control problem of spacecraft formation flying (SFF) system subject to uncertain mass and external perturbations. First, a general unified structure is proposed to represent the adjustable performance functions like the exponentially and appointed-time convergent ones. Then, an adaptive coordinated controller is developed based on a two-layer performance envelope to characterize the transient and steady-state formation maneuvering behaviors quantitatively of SFF system. Compared with the existing coordinated control approaches, the prominent advantage of the proposed one is that the preassigned position tracking and consensus tracking performance is guaranteed simultaneously while maintaining the scheduled formation configuration. Meanwhile, the users can configure and adjust the convergence rate (like the exponential or finite-time convergence) of the formation tracking errors by choosing different parameters arbitrarily in the unified structure for the performance functions. Finally, a group of numerical examples are organized to validated the effectiveness of the proposed coordinated control approach.

INDEX TERMS Spacecraft formation flying, prescribed performance control, formation maneuvers, finite-time control, coordinated control.

I. INTRODUCTION

The past few decades have witnessed the prosperous development of the spacecraft formation flying (SFF) system owing to its widespread application to various space missions such as earth observation, gravitational field mapping and on-orbit distributed sensing, to just name a few [1]–[3]. In light of the lower mission cost and higher performance as well as flexibility compared with a traditional monolithic spacecraft, the SFF system has attracted considerable attention and numerous outstanding contributions to this field have been established in the existing works. For example, a comprehensive survey on the guidance navigation and control requirements for the SFF system was presented in Ref. [4]. A detailed review of the modeling approaches and some newly developed state feedback controller design for the SFF system was given in Ref. [5].

In the SFF system, one key problem is how to maintain an accurate scheduled formation configuration when implementing a sequence of on-orbit formation maneuvers. To tackle this problem, many effective coordinated control approaches have been developed in the existing researches. Wherein, a distributed formation or containment control algorithm was devised for the leader and follower spacecraft, respectively, in the SFF system with consideration of multiple leader spacecraft and multiple follower spacecraft [6]. A continuous-time feedback tracking control scheme was designed to perform a formation maneuver of the SFF system via exploring a virtual leader state trajectory to avoid decentralized collisions [7]. To reconfigure and maintain a rigid formation while avoiding collisions between spacecraft, the Null-Space Based (NSB) concept was applied to formulate a behavioral control solution to the formation tracking control problem [8]. Moreover, the NSB was further developed to build a behavioral position coordinated control architecture for the SFF system with one leader spacecraft [9]. To remove the negative effects of the time delays, a relative position coordinated control scheme was given for the SFF system via exploring the backstepping control technique [10]. With consideration of negative effects induced

The associate editor coordinating the review of this manuscript and approving it for publication was Sun Junwei.

by the undesired uncertainties and external disturbances on the formation tracking accuracy, sliding mode control (SMC) technique has been widely applied to improve the robustness performance of the relevant coordinated controller like in Refs. [11] and [12]. By exploring the adaptive technique and finite-time stability theory, a nonsingular SMC controller was devised to guarantee the real combination synchronization of three complex-variable chaotic systems within finite time in Ref. [13]. To accelerate the convergence rate of the formation tracking error system, a unified synchronization framework with application to precision formation flying spacecraft was proposed in Ref. [14], wherein, the global exponential convergence rate could be achieved. In recent years, finite-time or fixed-time coordinated control approach for the SFF system has attracted wide attention owing to its faster convergence rate compared with the other ones mentioned above [15]. For example, a finite-time relative position coordinated tracking controller was derived by state feedback for the SFF system subject to unknown velocity information in Ref. [16]. A novel fixed-time coordinated controller was developed along with the artificial potential function to avoid the formation collisions based on the terminal SMC technique in Ref. [17]. In Ref. [18], a practical finite-time consensus controller was devised for the second-order heterogeneous switched nonlinear multi-agent system with consideration of different subsystem structures and the switching signals. To achieve the finite-time or fixed-time stability, fractional state feedback technique and symbolic functions are widely used in the foregoing research works. Although effective, the forms of the corresponding coordinated controllers are often tedious and the symbolic functions easily render the developed coordinated control schemes discontinuous. Moreover, to the authors' best knowledge, very few works center on guaranteeing the transient and steady-state formation tracking behaviors of the SFF system simultaneously.

To guarantee the tracking performance of the coordinated control approaches, prescribed performance control (PPC) theory proposed by Bechlioulis and Rovithakis provided a potential way, wherein, the convergence rate and steady-state behaviors of the controlled systems can be characterized quantitatively [19], [20]. Owing to the prominent advantage in predefining the transient and steady-state performance related to the practical requirements, PPC theory has been applied to develop the relevant control schemes for servo mechanisms, underwater acoustic sensor networks and MEMS gyroscope [21]–[23]. Moreover, attitude stabilization and tracking control problems with guaranteed performance were investigated in Refs. [24]–[26], in which the attitude constraints brought by the sensing instruments can be handled in the PPC structure. Ref. [27] extended the PPC theory to design an anti-saturated relative attitude and position tracking controller for the noncooperative spacecraft proximity operation. To solve the decentralized leader-follower formation tracking problem of a group of fully actuated unmanned surface vehicles (USVs), Ref. [28] attempted to use PPC theory to deal with the performance constraints on formation tracking errors during the USVs maneuvers. In the aforementioned PPC based works, the performance functions are often expressed by the exponential form, i.e., exponentially convergent stability can be obtained. To accelerate the convergence rate, by combing the finite-time technique mentioned above, finite-time PPC approaches have sprung up in the existing works like Refs. [29] and [30]. Wherein, the state performance constraints are dealt with the PPC structure, and the relevant finite-time controller is designed based on the fractional state feedback technique and symbolic functions. Thus, the inherent limitations like complex forms and discontinuous phenomenon of the developed controller mentioned above cannot be avoided. To tackle this problem, appointed-time convergent performance function concept was first proposed in Ref. [31], with which the appointed-time convergent controller can be derived based on the Lyapunov theory in the PPC structure. Compared with the traditional finite-time or fixed-time control approaches, the fractional state feedback technique and symbolic functions are avoided. Due to this advantage, appointed-time convergent performance function has been extended to various engineering applications such as the spacecraft attitude system and flexible air-breathing hypersonic vehicles [32], [33]. Although effective, there is lack of a unified form to involve the potential performance functions, which makes it difficult for the users to improve the control performance by configuring some appropriate parameters. Namely, the users are not easy to adjust the tracking performance of the controlled systems by choosing different performance functions, which is disadvantaged to the performance improvement especially for the high-precise requirements of the on-orbit formation maneuvers. Moreover, the uncertain dynamics and inherent nonlinearities are often encountered in practice. To solve this problem, neural networks and fuzzy systems are widely used to approximate the known nonlinear dynamics due to their universal approximation capabilities. Some relevant latest works can be found in Refs. [34]–[39] and references therein. Thus, it deserves further investigations on the coordinated control of the SFF systems with adjustable performance.

Inspired by the foregoing observations, this paper attempts to develop a novel coordinated control approach for the SFF system. For overcoming the limitation that there is no unified form for the existing performance functions in the PPC structure, we attempt to proposed a general form in which the users can configure the tracking performance freely. To guarantee the position tracking performance and consensus tracking performance simultaneously, a two-layer performance envelope is designed for the SFF system. Compared with the existing works, the main contributions are summarized as follows.

(1) A unified structure for the adjustable performance functions is first proposed, with which the exponential and finite-time or fixed-time performance functions can be at least expressed. Namely, the users can

configure and adjust the convergence rate (like the exponential or finite-time convergence) of the formation tracking performance by choosing different parameters in this unified structure easily;

(2) An adaptive coordinated control approach is developed based on the unified structure of the performance functions for the SFF system subject to unknown external perturbations and uncertain mass changes. Wherein, it is the first time that the two-layer control performance, i.e., the position tracking performance of each spacecraft and consensus tracking performance among the multiple spacecraft, can be guaranteed simultaneously under the devised controller.

The remainder of this paper is organized as follows. Sec. 2 presents the problem statement and preliminaries, wherein, the relative orbital dynamics of the SFF system and the preliminary knowledge of the graph theory are introduced. The main results on the adjustable performance function and coordinated controller are given in Sec. 3. A group of numerical examples are organized in Sec. 4. Some conclusions are drawn in Sec. 5.

Notations: $\|\cdot\|_1$ and $\|\cdot\|$ represents the 1-norm and Euclidean norm of a vector, respectively. T and $|\cdot|$ denote the vector transpose and absolute value of a scalar, respectively. $\mathcal{L}^\infty$ is a function set with its elements being essentially bounded measurable functions. Additionally, $\mathbb{R}^{m\times n}$ is a set of $m \times n$ real matrix.

II. PROBLEM STATEMENT AND PRELIMINARIES

A. RELATIVE ORBITAL DYNAMICS OF THE SFF SYSTEM

Without loss of generality, it is assumed that there are N spacecraft in the SFF system. Fig.1(a) illustrates the coordinate frames and relative positions among the multiple spacecraft based on Ref. [40]. Wherein, $\mathcal{FR}_0 = \{x_0, y_0, z_0\}$ denotes the earth-centered-inertial (ECI) frame with its origin being the mass of the earth. $\mathcal{FR}_c = \{x_c, y_c, z_c\}$ is the local-vertical-local-horizon (LVLH) reference frame, which is attached to a virtual reference spacecraft. When the virtual reference spacecraft locates in an elliptical orbit, then the position vector of the reference spacecraft is defined as $\boldsymbol{R}_c = [R_c, 0, 0]^{\mathrm{T}}$ in the LVLH frame with $R_c = a_c\left(1-e_c^2\right)/\left(1+e_c\cos\theta_c\right)$. Wherein, a_c, e_c, θ_c are, respectively, the semimajor axis, orbit eccentricity and true anomaly. For the i th spacecraft, its relative position and velocity vectors with respect to the virtual reference spacecraft are defined as $\boldsymbol{p}_i = [x_i, y_i, z_i]^{\mathrm{T}}$ and $\boldsymbol{v}_i = \left[v_{xi}, v_{yi}, v_{zi}\right]^{\mathrm{T}}$, respectively $(i = 1, 2, \ldots, N)$ in the LVLH frame. Accordingly, the relative orbital dynamic model is expressed by [40]

$$\begin{cases} \dot{\boldsymbol{p}}_i = \boldsymbol{v}_i \\ m_i\dot{\boldsymbol{v}}_i = \boldsymbol{u}_i + \boldsymbol{d}_i - \boldsymbol{C}_i\left(\dot{\theta}_c\right)\boldsymbol{v}_i \\ -\boldsymbol{D}_i\left(\dot{\theta}_c, \ddot{\theta}_c, R_i\right)\boldsymbol{p}_i - \boldsymbol{n}_i\left(R_i, R_c\right) \end{cases} \tag{1}$$

where $R_i = \sqrt{(R_c+x_i)^2+y_i^2+z_i^2}$, m_i is the mass of the i th spacecraft. $\boldsymbol{u}_i$ and $\boldsymbol{d}_i$ represent the actuator force and space perturbation, respectively. $\boldsymbol{C}_i(\cdot)$, $\boldsymbol{D}_i(\cdot)$, $\boldsymbol{n}_i(\cdot)$ are, respectively, the Coriolis-like skew-symmetric matrix, a time-varying potential force vector and gravity vector with the following detailed forms:

$$\begin{aligned} \boldsymbol{C}_i(\cdot) &= 2m_i\begin{bmatrix} 0 & -\dot{\theta}_c & 0 \\ \dot{\theta}_c & 0 & 0 \\ 0 & 0 & 0 \end{bmatrix} \\ \boldsymbol{n}_i(\cdot) &= m_i\mu\begin{bmatrix} R_c/R_i^3 - 1/R_c^2 \\ 0 \\ 0 \end{bmatrix} \\ \boldsymbol{D}_i(\cdot) &= m_i\begin{bmatrix} \mu/R_i^3 - \dot{\theta}_c^2 & -\ddot{\theta}_c & 0 \\ \ddot{\theta}_c & \mu/R_i^3 - \dot{\theta}_c^2 & 0 \\ 0 & 0 & \mu/R_i^3 \end{bmatrix} \end{aligned} \tag{2}$$

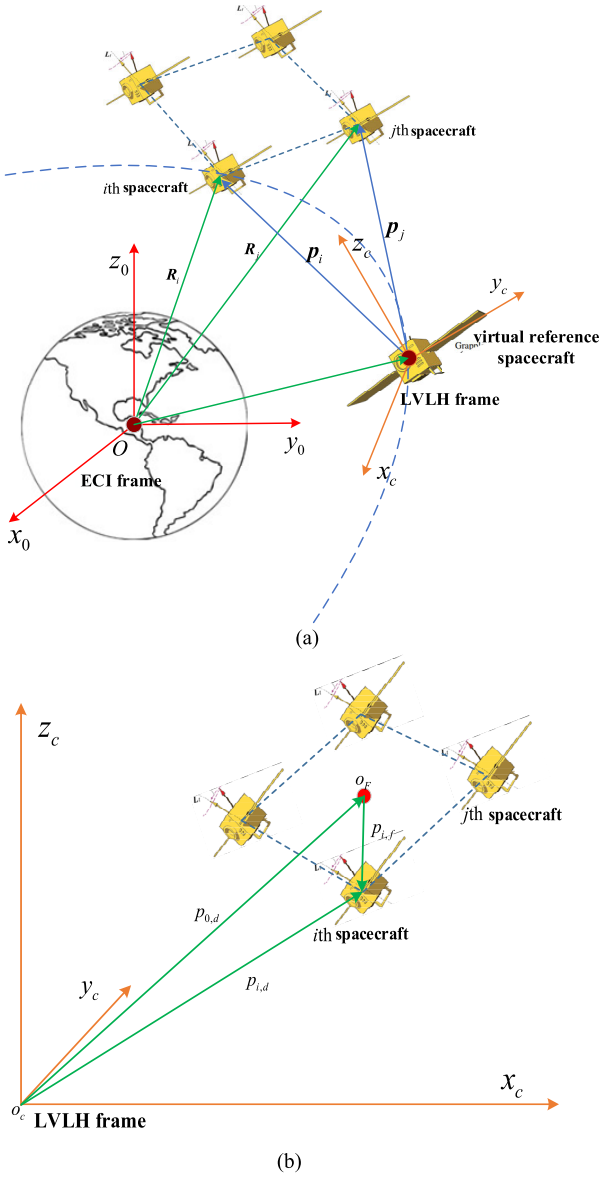

FIGURE 1. Sketch of the SFF system and the associated frames.

where μ is the geocentric gravitational constant. The true anomaly θ_c can be derived by the following equation:

$$\begin{cases} \dot{\theta}_c = \omega_c \left(1 - e_c \cos\theta_c\right)^2 / \left(1 - e_c^2\right)^{3/2} \\ \ddot{\theta}_c = -2\omega_c^2 e_c \left(1 + e_c \cos\theta_c\right)^3 \sin\theta_c / \left(1 - e_c^2\right)^3 \end{cases} \tag{3}$$

where $\omega_c = \sqrt{\mu / a_c^3}$ denotes the average orbital angular velocity.

Before moving, some preliminary knowledge of the graph theory is introduced as follows.

B. PRELIMINARIES OF THE GRAPH THEORY

For the N spacecraft in the SFF system, the relevant communication topology can be described by an undirected graph $\mathcal{G} = (\mathcal{V}, \mathcal{E})$ (without self-loop wireless communication), wherein, $\mathcal{V} = \{\mathcal{V}_1, \ldots, \mathcal{V}_N\}$ is the node set and each node represents the spacecraft. $\mathcal{E} \subseteq \mathcal{V} \times \mathcal{V}$ is the set of all edges. The adjacent matrix of graph $\mathcal{G}$ is defined as $\boldsymbol{A} = \left[a_{ij}\right] \in \mathbb{R}^{N \times N}$ with $a_{ij} \in \{0, 1\}$ being the weight of the matrix. If $\left(\mathcal{V}_i, \mathcal{V}_j\right) \in \mathcal{E}$, then $a_{ij} = 1$, otherwise, $a_{ij} = 0\,(i, j = 1, \ldots, N)$. For the i th node $\mathcal{V}_i$, its adjacent node set is defined as $\mathcal{N}_i = \left\{j \middle| \left(\mathcal{V}_i, \mathcal{V}_j\right) \in \mathcal{E}\right\}$. Accordingly, the in-degree matrix of the graph $\mathcal{G}$ is $\boldsymbol{B} = \text{diag}\{B_1, \ldots, B_N\}$ with $B_i = \sum_{j \in \mathcal{N}_i} a_{ij}$. Then, the Laplacian matrix $\boldsymbol{L}$ of the graph $\mathcal{G}$ is obtained as $\boldsymbol{L} = \left[\ell_{ij}\right] = \boldsymbol{B} - \boldsymbol{A}$ with $\ell_{ii} = \sum_{i=1}^{N} a_{ij}$ and $\ell_{ij} = -a_{ij}\,(i \neq j)$.

In this paper, to facilitate the subsequent controller design, two assumptions are imposed for the SFF system.

Assumption 1: For i th spacecraft, its mass is unknown but bounded with slow change rate.

Assumption 2: The space perturbation $\boldsymbol{d}_i$ is unknown but bounded and satisfies $\|\boldsymbol{d}_i\| \leq d_{i,0}$ with $d_{i,0}$ being a positive constant.

Remark 1: With consideration of the fuel consumption and the complex space environment, the foregoing two assumptions are reasonable, which can be founded in the existing works like Refs. [10], [14], and [40].

Based on the aforementioned discussions, the control objective of this work is summarized as:

(1) Each spacecraft in the SFF system can track the desired position under the devised controller while the scheduled formation configuration is preserved.
(2) The tracking performance (like the convergence rate and steady-state tracking errors) can be configured by the users.

III. MAIN RESULTS

A. ADJUSTABLE PERFORMANCE FUNCTION DESIGN

Before devising the relevant controller during formation-keeping maneuvers, an adjustable performance function is formulated with the following detailed form:

$$\dot{\rho}\,(t) = -\varphi\left(\rho\,(t)\right), \quad \rho\,(0) = \rho_0 > 0 \tag{4}$$

where $\rho\,(t)$ is the adjustable performance function defined on the set $[0, \infty)$. $\varphi\,(\cdot)$ is a $\mathcal{K}_\infty$-type function with respect to $\rho\,(t)$ and is locally Lipschitz continuous. Generally, different type of $\varphi\,(\cdot)$ will lead to different adjustable performance function $\rho\,(t)$. In practice, the tracking accuracy can be set as the equilibrium point of function $\varphi\,(\cdot)$.

For the convergence rate, it can be configured freely by the users to choose different parameters of function $\varphi\,(\cdot)$.

For the defined adjustable performance function, the following property holds.

Property 1: If Eq. (4), holds, then $\rho\,(t) \in \mathcal{L}^\infty\,[0, \infty]$ and satisfies $\lim_{t \to \infty} \rho\,(t) = 0$.

Proof: The proof of *Property 1* is organized as follows. First, construct the following Lyapunov function:

$$V_\rho = \frac{1}{2}\rho^2\,(t) \tag{5}$$

Taking the time-derivative of V_ρ yields $\dot{V}_\rho = \rho\,(t)\,\dot{\rho}\,(t)$. Substituting Eq. (4) into $\dot{V}_\rho$ gets $\dot{V}_\rho = -\rho\,(t)\,\varphi\left(\rho\,(t)\right)$. Because $\varphi\,(\cdot)$ is a $\mathcal{K}_\infty$-type function with respect to $\rho\,(t)$, one can obtain $\dot{V}_\rho < 0$. Consequently, $\rho\,(t)$ is monotonically decreasing and satisfies $\lim_{t \to \infty} \rho\,(t) = 0, \ \forall t \in [0, \infty)$. Namely, $\rho\,(t) \in \mathcal{L}^\infty\,[0, \infty]$ and $\lim_{t \to \infty} \rho\,(t) = 0$. Thereby, the proof of *Property 1* is completed. ■

Remark 2: Based on Eq. (4), one can construct different adjustable performance function $\rho\,(t)$ when choosing different $\mathcal{K}_\infty$-type function $\varphi\,(\cdot)$. For example, when $\varphi\left(\rho\,(t)\right) = c_0\rho\,(t)\ \ (c_0 > 0)$, based on Eq. (4), one can find that the corresponding performance function $\rho\,(t)$ is exponentially convergent. When $\varphi\left(\rho\,(t)\right) = c_0\left(\rho\,(t) - \rho_\infty\right)^\eta$, one can obtain that the derived performance function $\rho\,(t)$ is finite-time convergent to the steady-state bound ρ_∞ ($\rho_0 > \rho_\infty$, $c_0 > 0$, $\eta \in (0, 1)$). The detailed proof of the foregoing discussions can be found in the authors' previous work in Ref. [31], which is omitted for brief. It is noteworthy that different $\mathcal{K}_\infty$ function $\varphi\,(\cdot)$ will influence the convergence and steady-state performance of the performance function $\rho\,(t)$. Namely, the performance of function $\rho\,(t)$ is adjustable by choosing different $\varphi\,(\cdot)$ and its parameters. Figure 2 presents the trajectories of the adjustable performance function under different $\mathcal{K}_\infty$-type functions.

B. ADAPTIVE COORDINATED CONTROLLER DESIGN BASED ON ADJUSTABLE PERFORMANCE FUNCTION

In this part, the adaptive coordinated controller will be designed based on the foregoing adjust-able performance function. Before moving, the following auxiliary state variable is defined for the i th spacecraft:

$$\boldsymbol{s}_i = \tilde{\boldsymbol{v}}_i + \boldsymbol{\gamma}_i\tilde{\boldsymbol{p}}_i = \left(\boldsymbol{v}_i - \boldsymbol{v}_{i,d}\right) + \boldsymbol{\gamma}_i\left(\boldsymbol{p}_i - \boldsymbol{p}_{i.d}\right) \tag{6}$$

where $\boldsymbol{\gamma}_i \in \mathbb{R}^{3\times3}$ is a positive-definite diagonal matrix. $\boldsymbol{p}_{i.d}, \boldsymbol{v}_{i,d}$ are, respectively, the desired position and velocity vectors with the following detailed forms:

$$\begin{cases} \boldsymbol{p}_{i,d} = \boldsymbol{p}_{0,d} + \boldsymbol{p}_{i,f} \\ \boldsymbol{v}_{i,d} = \dot{\boldsymbol{p}}_{i,d} \end{cases} \tag{7}$$

where $\boldsymbol{p}_{0,d}, \boldsymbol{p}_{i,f}$ denote the desired position of the formation center and the desired position of the i th spacecraft with

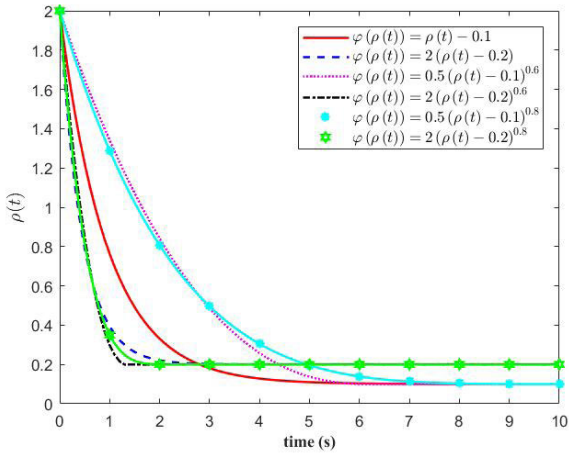

FIGURE 2. Trajectories of the adjustable performance function under different $\mathcal{K}_\infty$-type functions.

respect the formation center, respectively, with the relevant geometrical descriptions being given in Fig.1(b). In practice, the formation center and the relative position with respect to the formation center can be accessed to each spacecraft. Thus, the above information $\boldsymbol{p}_{i,d}$, $\boldsymbol{v}_{i,d}$ is known for each spacecraft.

To quantitatively characterize the tracking control performance during formation-keeping maneuvers, for the k th dimensional element of $\boldsymbol{s}_i$ $(k = 1, 2, 3)$, the following performance envelope is predefined:

$$-\underline{\delta}_{s,ik}\rho_{s,i}(t) < s_{ik} < -\bar{\delta}_{s,ik}\rho_{s,i}(t) \quad (k = 1, 2, 3) \tag{8}$$

where $\underline{\delta}_{s,ik}, \bar{\delta}_{s,ik} \in (0, 1]$ are constants. $\rho_{s,i}(t)$ is the adjustable performance function derived from Eq. (4). To achieve the consensus control among the spacecraft in the SFF system, the following consensus error is defined:

$$\boldsymbol{e}_{s,ij} = \boldsymbol{s}_i - \boldsymbol{s}_j \tag{9}$$

Similar with Eq. (10), the performance envelope for consensus error $\boldsymbol{e}_{s,ij}$ is defined as:

$$-\underline{\delta}_{e,ijk}\rho_{e,ij}(t) < e_{s,ijk} = s_{ik} - s_{jk} < \bar{\delta}_{e,ijk}\rho_{e,ij}(t) \tag{10}$$

where $\underline{\delta}_{e,ijk}, \bar{\delta}_{e,ijk} \in (0, 1]$ $(k = 1, 2, 3)$ are constants. $\rho_{e,ij}(t)$ is the adjustable performance function derived from Eq. (4).

Remark 3: With consideration of $\boldsymbol{e}_{s,ij} = \boldsymbol{s}_i - \boldsymbol{s}_j$ and $\boldsymbol{e}_{s,ji} = \boldsymbol{s}_j - \boldsymbol{s}_i$, for the consensus error $\boldsymbol{e}_{s,ji}$, its performance envelope can be designed as $-\underline{\delta}_{e,jik}\rho_{e,ji}(t) < e_{s,jik} = s_{jk} - s_{ik} < \bar{\delta}_{e,jik}\rho_{e,ji}(t)$ with $\underline{\delta}_{e,jik} = \bar{\delta}_{e,ijk}$, $\bar{\delta}_{e,jik} = \underline{\delta}_{e,ijk}$, $\rho_{e,ji}(t) = \rho_{e,ij}(t)$.

To facilitate the subsequent controller design, based on Eq. (8) and (10), the following standard tracking errors are defined as:

$$\omega_{s,ik} = \frac{s_{ik}}{\rho_{s,i}(t)}, \quad \omega_{e,ijk} = \frac{e_{s,ijk}}{\rho_{e,ij}(t)} \tag{11}$$

Based on the aforementioned analysis, the adaptive coordinated controller for the i th spacecraft is devised as:

$$\begin{cases} \boldsymbol{u}_i = \underbrace{-k_{1,i}\boldsymbol{\eta}_{s,i}\boldsymbol{z}_{s,i} - k_{2,i}\sum_{j\in\mathcal{N}_i} a_{ij}\boldsymbol{\eta}_{e,ij}\boldsymbol{z}_{e,ij}}_{formationtracking\ controller} \\ \quad \underbrace{-\hat{m}_i\boldsymbol{\varphi}_i\left(\boldsymbol{p}_i, \boldsymbol{p}_{i,d}, \boldsymbol{v}_i, \boldsymbol{v}_{i,d}\right)}_{nonlinear\ compensation\ controller} \\ \quad -\boldsymbol{u}_{dr,i} \\ disturbance\ rejection\ controller \\ u_{dr,ik} = \begin{cases} \frac{s_{ik}}{|s_{ik}|}\hat{d}_{i,0}, & |s_{ik}| \geq \varepsilon_{i,0} \\ \frac{s_{ik}}{\varepsilon_{i,0}^2}\hat{d}_{i,0}^2, & |s_{ik}| < \varepsilon_{i,0} \end{cases} \\ \boldsymbol{\varphi}_i\left(\boldsymbol{p}_i, \boldsymbol{p}_{i,d}, \boldsymbol{v}_i, \boldsymbol{v}_{i,d}\right) \\ = -\left(\boldsymbol{C}_i\left(\dot{\theta}_c\right)\boldsymbol{v}_i + \boldsymbol{D}_i\left(\dot{\theta}_c, \ddot{\theta}_c, R_i\right)\boldsymbol{p}_i + \boldsymbol{n}_i\left(R_i, R_c\right)\right)/m_i \\ -\dot{\boldsymbol{v}}_{i,d} + \boldsymbol{\gamma}_i\left(\boldsymbol{v}_i - \boldsymbol{v}_{i.d}\right) \end{cases} \tag{12}$$

where $k_{1,i}, k_{2,i} \in \mathbb{R}$ are positive control gains. $\hat{m}_i$ is the estimated mass value of the i th spacecraft. $\hat{d}_{i,0}$ is the estimated value for the unknown space perturbations. $\boldsymbol{u}_{dr,i} = \left[u_{dr,i1}, u_{dr,i2}, u_{dr,i3}\right]^{\mathrm{T}}$ is the robust controller for disturbance rejection. $\varepsilon_{i,0} > 0$ is a small positive constant. $\boldsymbol{z}_{s,i} = \left[z_{s,i1}, z_{s,i2}, z_{s,i3}\right]^{\mathrm{T}}$, $\boldsymbol{z}_{e,ij} = \left[z_{e,ij1}, z_{e,ij2}, z_{e,ij3}\right]^{\mathrm{T}}$, $\boldsymbol{\eta}_{s,i} = \mathrm{diag}\left\{\eta_{s,i1}, \eta_{s,i2}, \eta_{s,i3}\right\}$ and $\boldsymbol{\eta}_{e,ij} = \mathrm{diag}\left\{\eta_{e,ij1}, \eta_{e,ij2}, \eta_{e,ij3}\right\}$ are the intermediate variables with its k th $(k = 1, 2, 3)$ dimensional element being expressed by

$$\begin{cases} z_{s,ik} = \ln\left(\dfrac{\underline{\delta}_{s,ik}\bar{\delta}_{s,ik} + \bar{\delta}_{s,ik}\omega_{s,ik}}{\underline{\delta}_{s,ik}\bar{\delta}_{s,ik} - \underline{\delta}_{s,ik}\omega_{s,ik}}\right) \\ z_{e,ijk} = \ln\left(\dfrac{\underline{\delta}_{e,ijk}\bar{\delta}_{e,ijk} + \bar{\delta}_{s,ijk}\omega_{e,ijk}}{\underline{\delta}_{e,ijk}\bar{\delta}_{e,ijk} - \underline{\delta}_{e,ijk}\omega_{e,ijk}}\right) \\ \eta_{s,ik} = \dfrac{\underline{\delta}_{s,ik}\bar{\delta}_{s,ik}}{\left(\omega_{s,ik} + \delta_{s,ik}\right)\left(\bar{\delta}_{s,ik} - \omega_{s,ik}\right)\left(\underline{\delta}_{s,ik} + \bar{\delta}_{s,ik}\right)\rho_{s,i}(t)} \\ \eta_{e,ijk} \\ = \dfrac{\underline{\delta}_{e,ijk}\bar{\delta}_{e,ijk}}{\left(\omega_{e,ijk} + \underline{\delta}_{e,ijk}\right)\left(\bar{\delta}_{e,ijk} - \omega_{e,ijk}\right)\left(\underline{\delta}_{e,ijk} + \bar{\delta}_{e,ijk}\right)\rho_{e,ij}(t)} \end{cases} \tag{13}$$

The adaptive schemes of $\hat{m}_i$ and k th $(k = 1, 2, 3)$ dimensional element $\hat{d}_{ik}$ are formulated as

$$\begin{cases} \dot{\hat{m}}_i = \kappa_{m,i}\boldsymbol{s}_i^{\mathrm{T}}\boldsymbol{\varphi}_i\left(\boldsymbol{p}_i, \boldsymbol{p}_{i,d}, \boldsymbol{v}_i, \boldsymbol{v}_{i,d}\right) \\ \dot{\hat{d}}_{i,0} = \kappa_{d,i}\left\|\boldsymbol{s}_i\right\|_1 \end{cases} \tag{14}$$

where $\kappa_{m,i}, \kappa_{d,i}$ are positive constants.

Remark 4: As shown in the Eq. (12), the adaptive coordinated controller is divided into three parts. The first is the formation tracking control term which is used to guarantee the preassigned transient and steady-state performance for the position tracking errors and consensus tracking errors. The second is the nonlinear compensation term which is used to weaken the negative effects brought by the nonlinearities. The third is the disturbance rejection term which is used to

improve the robustness of the controller with respect to the external disturbance. The reason that the disturbance rejection term is designed in such form is to avoid the chattering phenomenon induced by the traditional disturbance rejection controller based on the symbolic functions.

According to the foregoing coordinated controller in Eq. (12) and adaptive scheme in Eq. (14), one important result of this paper is summarized in the following theorem.

Theorem 1: *Each spacecraft in the SFF system can track its desired position with guaranteed coordinated control performance while maintaining the schedule formation configuration under the devised coordinated controller in Eq. (12) and adaptive scheme in Eq. (14). Moreover, all the close-loop signals are uniformly ultimately bounded.*

Proof: The proof of *Theorem 1* is organized as follows. First, construct the following Lyapunov function V_1:

$$V_1 = \frac{1}{2}\sum_{i=1}^{N} m_i \boldsymbol{s}_i^{\mathrm{T}} \boldsymbol{s}_i \tag{15}$$

Taking the time-derivative of V_1 gets

$$\dot{V}_1 = \sum_{i=1}^{N} m_i \boldsymbol{s}_i^{\mathrm{T}} \dot{\boldsymbol{s}}_i \tag{16}$$

Based on Eq. (1) and (6), the detailed form of $\dot{\boldsymbol{s}}_i$ is expressed by

$$\begin{aligned}\dot{\boldsymbol{s}}_i &= \dot{\tilde{\boldsymbol{v}}}_i + \boldsymbol{\gamma}_i \dot{\tilde{\boldsymbol{p}}}_i = \left(\dot{\boldsymbol{v}}_i - \dot{\boldsymbol{v}}_{i,d}\right) + \boldsymbol{\gamma}_i \left(\dot{\boldsymbol{p}}_i - \dot{\boldsymbol{p}}_{i.d}\right) \\ &= \frac{1}{m_i}\left[\boldsymbol{u}_i + \boldsymbol{d}_i - \boldsymbol{C}_i\left(\dot{\theta}_c\right)\boldsymbol{v}_i - \boldsymbol{D}_i\left(\dot{\theta}_c, \ddot{\theta}_c, R_i\right)\boldsymbol{p}_i - \boldsymbol{n}_i\left(R_i, R_c\right)\right] \\ &\quad - \dot{\boldsymbol{v}}_{i,d} + \boldsymbol{\gamma}_i\left(\boldsymbol{v}_i - \boldsymbol{v}_{i.d}\right)\end{aligned} \tag{17}$$

Substituting Eqs. (12) and (13) into (17) yields

$$\begin{aligned} m_i\dot{\boldsymbol{s}}_i &= \boldsymbol{u}_i + \boldsymbol{d}_i - \boldsymbol{C}_i\left(\dot{\theta}_c\right)\boldsymbol{v}_i - \boldsymbol{D}_i\left(\dot{\theta}_c, \ddot{\theta}_c, R_i\right)\dot{\boldsymbol{p}}_i - \boldsymbol{n}_i\left(R_i, R_c\right) \\ &\quad + m_i\left(-\dot{\boldsymbol{v}}_{i,d} + \boldsymbol{\gamma}_i\left(\boldsymbol{v}_i - \boldsymbol{v}_{i.d}\right)\right) \\ &= \boldsymbol{u}_i + \boldsymbol{d}_i + m_i\boldsymbol{\varphi}\left(\boldsymbol{p}_i, \boldsymbol{p}_{i,d}, \boldsymbol{v}_i, \boldsymbol{v}_{i,d}\right) \\ &= -k_{1,i}\boldsymbol{\eta}_{s,i}\boldsymbol{z}_{s,i} - k_{2,i}\sum_{j\in\mathcal{N}_i} a_{ij}\boldsymbol{\eta}_{e,ij}\boldsymbol{z}_{e,ij} \\ &\quad - \hat{m}_i\boldsymbol{\varphi}_i\left(\boldsymbol{p}_i, \boldsymbol{p}_{i,d}, \boldsymbol{v}_i, \boldsymbol{v}_{i,d}\right) \\ &\quad - \boldsymbol{u}_{dr,i} + \boldsymbol{d}_i + m_i\boldsymbol{\varphi}\left(\boldsymbol{p}_i, \boldsymbol{p}_{i,d}, \boldsymbol{v}_i, \boldsymbol{v}_{i,d}\right) \\ &= -k_{1,i}\boldsymbol{\eta}_{s,i}\boldsymbol{z}_{s,i} - k_{2,i}\sum_{j\in\mathcal{N}_i} a_{ij}\boldsymbol{\eta}_{e,ij}\boldsymbol{z}_{e,ij} - \boldsymbol{u}_{dr,i} \\ &\quad + \left(m_i - \hat{m}_i\right)\boldsymbol{\varphi}_i\left(\boldsymbol{p}_i, \boldsymbol{p}_{i,d}, \boldsymbol{v}_i, \boldsymbol{v}_{i,d}\right) + \boldsymbol{d}_i \\ &= -k_{1,i}\boldsymbol{\eta}_{s,i}\boldsymbol{z}_{s,i} - k_{2,i}\sum_{j\in\mathcal{N}_i} a_{ij}\boldsymbol{\eta}_{e,ij}\boldsymbol{z}_{e,ij} - \boldsymbol{u}_{dr,i} \\ &\quad + \tilde{m}_i\boldsymbol{\varphi}_i\left(\boldsymbol{p}_i, \boldsymbol{p}_{i,d}, \boldsymbol{v}_i, \boldsymbol{v}_{i,d}\right) + \boldsymbol{d}_i \end{aligned} \tag{18}$$

Accordingly, Eq. (16) becomes

$$\begin{aligned}\sum_{i=1}^{N} m_i\boldsymbol{s}_i^{\mathrm{T}}\dot{\boldsymbol{s}}_i &= -k_{1,i}\boldsymbol{s}_i^{\mathrm{T}}\boldsymbol{\eta}_{s,i}\boldsymbol{z}_{s,i} - k_{2,i}\boldsymbol{s}_i^{\mathrm{T}}\sum_{j\in\mathcal{N}_i} a_{ij}\boldsymbol{\eta}_{e,ij}\boldsymbol{z}_{e,ij} \\ &\quad + \tilde{m}_i\boldsymbol{s}_i^{\mathrm{T}}\boldsymbol{\varphi}_i\left(\boldsymbol{p}_i, \boldsymbol{p}_{i,d}, \boldsymbol{v}_i, \boldsymbol{v}_{i,d}\right) - \boldsymbol{s}_i^{\mathrm{T}}\boldsymbol{u}_{dr,i} + \boldsymbol{s}_i^{\mathrm{T}}\boldsymbol{d}_i\end{aligned} \tag{19}$$

Based on Eq. (13), the k th dimensional element of $-k_{1,i}\boldsymbol{s}_i^{\mathrm{T}}\boldsymbol{\eta}_{s,i}\boldsymbol{z}_{s,i}$ can be expanded as

$$\begin{aligned} &-k_{1,i}s_{ik}\eta_{s,ik}z_{s,ik} \\ &= -\frac{k_{1,i}\underline{\delta}_{s,ik}\bar{\delta}_{s,ik}s_{ik}}{\left(\omega_{s,ik} + \underline{\delta}_{s,ik}\right)\left(\omega_{s,ik} - \bar{\delta}_{s,ik}\right)\left(\underline{\delta}_{s,ik} + \bar{\delta}_{s,ik}\right)\rho_{s,i}\left(t\right)}z_{s,ik} \\ &= -k_{1,i}\xi_{s,ik}\omega_{s,ik}\ln\left(\frac{\underline{\delta}_{s,ik}\bar{\delta}_{s,ik} + \bar{\delta}_{s,ik}\omega_{s,ik}}{\underline{\delta}_{s,ik}\bar{\delta}_{s,ik} - \underline{\delta}_{s,ik}\omega_{s,ik}}\right) \\ &= -k_{1,i}\xi_{s,ik}\omega_{s,ik}^2\phi\left(\omega_{s,ik}\right) \end{aligned} \tag{20}$$

where $\xi_{s,ik}$, $\phi\left(\omega_{s,ik}\right)$ are given by

$$\begin{cases} \xi_{s,ik} = \dfrac{\underline{\delta}_{s,ik}\bar{\delta}_{s,ik}}{\left(\underline{\delta}_{s,ik} + \bar{\delta}_{s,ik}\right)\left(\omega_{s,ik} + \underline{\delta}_{s,ik}\right)\left(\bar{\delta}_{s,ik} - \omega_{s,ik}\right)} \\ \phi\left(\omega_{s,ik}\right) = \dfrac{1}{\omega_{s,ik}}\ln\left(\dfrac{\underline{\delta}_{s,ik}\bar{\delta}_{s,ik} + \bar{\delta}_{s,ik}\omega_{s,ik}}{\underline{\delta}_{s,ik}\bar{\delta}_{s,ik} - \underline{\delta}_{s,ik}\omega_{s,ik}}\right) \end{cases} \tag{21}$$

Taking $\phi\left(\omega_{s,ik}\right)$ with respect to $\omega_{s,ik}$ gets

$$\begin{aligned}\phi\left(\omega_{s,ik}\right) &= \frac{\mathrm{d}\phi\left(\omega_{s,ik}\right)}{\mathrm{d}\omega_{s,ik}} \\ &= \frac{1}{\omega_{s,ik}}\left[\frac{\bar{\delta}_{s,ik} + \underline{\delta}_{s,ik}}{\left(\omega_{s,ik} + \underline{\delta}_{s,ik}\right)\left(\bar{\delta}_{s,ik} - \omega_{s,ik}\right)}\right. \\ &\quad \left. - \frac{1}{\omega_{s,ik}}\ln\left(\frac{\bar{\delta}_{s,ik}\underline{\delta}_{s,ik} + \bar{\delta}_{s,ik}\omega_{s,ik}}{\bar{\delta}_{s,ik}\underline{\delta}_{s,ik} - \underline{\delta}_{s,ik}\omega_{s,ik}}\right)\right]\end{aligned} \tag{22}$$

Based on Eq. (8), one can find that when $0 < \omega_{s,ik} < \bar{\delta}_{s,ik}$, $\phi\left(\omega_{s,ik}\right) > 0$ and $-\underline{\delta}_{s,ik} < \omega_{s,ik} < 0$, $\phi\left(\omega_{s,ik}\right) < 0$. Thus, by applying L'Hopital's rule, one can obtain that the minimal value of $\phi\left(\omega_{s,ik}\right)$ on the set $\left(-\underline{\delta}_{s,ik}, \bar{\delta}_{s,ik}\right)$, i.e., it is:

$$\begin{aligned}\phi_{\min}\left(\omega_{s,ik}\right) &= \lim_{\omega_{s,ik}\to 0^+}\phi_{\min}\left(\omega_{s,ik}\right) \\ &= \lim_{\omega_{s,ik}\to 0^-}\phi_{\min}\left(\omega_{s,ik}\right) = \left.\frac{\mathrm{d}z_{s,ik}/\mathrm{d}\omega_{s,ik}}{1}\right|_{\omega_{s,ik}=0} \\ &= \left.\frac{\bar{\delta}_{s,ik} + \underline{\delta}_{s,ik}}{\left(\omega_{s,ik} + \underline{\delta}_{s,ik}\right)\left(\bar{\delta}_{s,ik} - \omega_{s,ik}\right)}\right|_{\omega_{s,ik}=0} \\ &= \frac{\bar{\delta}_{s,ik} + \delta_{s,ik}}{\bar{\delta}_{s,ik}\underline{\delta}_{s,ik}}\end{aligned} \tag{23}$$

Substituting Eq. (23) into (20) yields

$$\begin{aligned}-k_{1,i}s_{ik}\eta_{s,ik}z_{s,ik} &\le -k_{1,i}\xi_{s,ik}\frac{\bar{\delta}_{s,ik} + \underline{\delta}_{s,ik}}{\bar{\delta}_{s,ik}\underline{\delta}_{s,ik}}\omega_{s,ik}^2 \\ &= \frac{-k_{1,i}}{\left(\omega_{s,ik} + \underline{\delta}_{s,ik}\right)\left(\bar{\delta}_{s,ik} - \omega_{s,ik}\right)}\omega_{s,ik}^2\end{aligned} \tag{24}$$

For the $-k_{2,i}\boldsymbol{s}_i^{\mathrm{T}}\sum_{j\in\mathcal{N}_i} a_{ij}\boldsymbol{\eta}_{e,ij}\boldsymbol{z}_{e,ij}$ in Eq. (19), its k th dimensional element satisfies

$$-k_{2,i}\sum_{i=1}^{N} s_{ik}\sum_{j\in\mathcal{N}_i} a_{ij}\eta_{e,ijk}z_{e,ijk}$$

$$= -k_{2,i}\sum_{i=1}^{N} s_{ik}\sum_{j\in\mathcal{N}_i} a_{ij}\eta_{e,ijk}z_{e,ijk}$$
$$= -k_{2,i}\sum_{i=1}^{N} s_{ik}\sum_{j\in\mathcal{N}_i} \frac{a_{ij}\xi_{e,ijk}}{\rho_{e,ij}(t)}\ln\left(\frac{\underline{\delta}_{e,ijk}\bar{\delta}_{e,ijk}+\bar{\delta}_{s,ijk}\omega_{e,ijk}}{\underline{\delta}_{e,ijk}\bar{\delta}_{e,ijk}-\underline{\delta}_{e,ijk}\omega_{e,ijk}}\right) \tag{25}$$

where $\xi_{e,ijk} = \frac{\underline{\delta}_{e,ijk}\bar{\delta}_{e,ijk}}{\left(\underline{\delta}_{e,ijk}+\bar{\delta}_{e,ijk}\right)\left(\omega_{e,ijk}+\underline{\delta}_{e,ijk}\right)\left(\bar{\delta}_{e,ijk}-\omega_{e,ijk}\right)}$. Based on *Remark 3*, one can obtain that

$$\ln\left(\frac{\underline{\delta}_{e,ijk}\bar{\delta}_{e,ijk}+\bar{\delta}_{e,ijk}\omega_{e,ijk}}{\underline{\delta}_{e,ijk}\bar{\delta}_{e,ijk}-\underline{\delta}_{e,ijk}\omega_{e,ijk}}\right)$$
$$= \ln\left(\frac{\bar{\delta}_{e,jik}\underline{\delta}_{e,jik}-\underline{\delta}_{e,ijk}\omega_{e,jik}}{\bar{\delta}_{e,jik}\underline{\delta}_{e,jik}+\bar{\delta}_{e,ijk}\omega_{e,jik}}\right)$$
$$= -\ln\left(\frac{\bar{\delta}_{e,jik}\underline{\delta}_{e,jik}+\bar{\delta}_{e,ijk}\omega_{e,jik}}{\bar{\delta}_{e,jik}\underline{\delta}_{e,jik}-\bar{\delta}_{e,ijk}\omega_{e,jik}}\right) \tag{26}$$

$$\xi_{e,ijk}$$
$$= \frac{\underline{\delta}_{e,ijk}\bar{\delta}_{e,ijk}}{\left(\underline{\delta}_{e,ijk}+\bar{\delta}_{e,ijk}\right)\left(\omega_{e,ijk}+\underline{\delta}_{e,ijk}\right)\left(\bar{\delta}_{e,ijk}-\omega_{e,ijk}\right)}$$
$$= \frac{\bar{\delta}_{e,jik}\underline{\delta}_{e,ijk}}{\left(\bar{\delta}_{e,jik}+\underline{\delta}_{e,jik}\right)\left(\bar{\delta}_{e,jik}-\omega_{e,jik}\right)\left(\omega_{e,jik}+\underline{\delta}_{e,jik}\right)} = \xi_{e,jik} \tag{27}$$

Based on Eqs. (10) and (11), $\rho_{e,ij}(t) = \rho_{e,ji}(t)$ and $a_{ij} = a_{ji}$ on an undirected graph, one can further obtain that

$$\frac{1}{2}\sum_{i=1}^{N}\sum_{j\in\mathcal{N}_i}\frac{a_{ij}\left(s_{ik}-s_{jk}\right)\xi_{e,ijk}}{\rho_{e,ij}(t)}\ln\left(\frac{\underline{\delta}_{e,ijk}\bar{\delta}_{e,ijk}+\bar{\delta}_{s,ijk}\omega_{e,ijk}}{\underline{\delta}_{e,ijk}\bar{\delta}_{e,ijk}-\underline{\delta}_{e,ijk}\omega_{e,ijk}}\right)$$
$$= \frac{1}{2}\sum_{i=1}^{N} s_{ik}\sum_{j\in\mathcal{N}_i}\frac{a_{ij}\xi_{e,ijk}}{\rho_{e,ij}(t)}\ln\left(\frac{\underline{\delta}_{e,ijk}\bar{\delta}_{e,ijk}+\bar{\delta}_{s,ijk}\omega_{e,ijk}}{\underline{\delta}_{e,ijk}\bar{\delta}_{e,ijk}-\underline{\delta}_{e,ijk}\omega_{e,ijk}}\right)$$
$$-\frac{1}{2}\sum_{i=1}^{N} s_{jk}\sum_{j\in\mathcal{N}_i}\frac{a_{ij}\xi_{e,ijk}}{\rho_{e,ij}(t)}\ln\left(\frac{\underline{\delta}_{e,ijk}\bar{\delta}_{e,ijk}+\bar{\delta}_{s,ijk}\omega_{e,ijk}}{\underline{\delta}_{e,ijk}\bar{\delta}_{e,ijk}-\underline{\delta}_{e,ijk}\omega_{e,ijk}}\right)$$
$$= \frac{1}{2}\sum_{i=1}^{N} s_{ik}\sum_{j\in\mathcal{N}_i}\frac{a_{ij}\xi_{e,ijk}}{\rho_{e,ij}(t)}\ln\left(\frac{\underline{\delta}_{e,ijk}\bar{\delta}_{e,ijk}+\bar{\delta}_{s,ijk}\omega_{e,ijk}}{\underline{\delta}_{e,ijk}\bar{\delta}_{e,ijk}-\underline{\delta}_{e,ijk}\omega_{e,ijk}}\right)$$
$$-\frac{1}{2}\sum_{j=1}^{N} s_{jk}\sum_{i\in\mathcal{N}_i}\frac{a_{ji}\xi_{e,jik}}{\rho_{e,ji}(t)}\ln\left(\frac{\underline{\delta}_{e,ijk}\bar{\delta}_{e,ijk}+\bar{\delta}_{s,ijk}\omega_{e,ijk}}{\underline{\delta}_{e,ijk}\bar{\delta}_{e,ijk}-\underline{\delta}_{e,ijk}\omega_{e,ijk}}\right)$$
$$= \sum_{i=1}^{N}\sum_{j\in\mathcal{N}_i}\frac{a_{ij}s_{ik}\xi_{e,ijk}}{\rho_{e,ij}(t)}\ln\left(\frac{\underline{\delta}_{e,ijk}\bar{\delta}_{e,ijk}+\bar{\delta}_{s,ijk}\omega_{e,ijk}}{\underline{\delta}_{e,ijk}\bar{\delta}_{e,ijk}-\underline{\delta}_{e,ijk}\omega_{e,ijk}}\right) \tag{28}$$

By comparing Eq. (20), one can find that Eq. (28) has the same configuration. Thus, similar with Eq. (24), one can obtain the following result:

$$-k_{2,i}\sum_{i=1}^{N} s_{ik}\sum_{j\in\mathcal{N}_i} a_{ij}\eta_{e,ijk}z_{e,ijk}$$
$$\le -k_{2,i}\sum_{i=1}^{N}\sum_{j\in\mathcal{N}_i}\frac{a_{ij}}{\left(\omega_{e,ijk}+\underline{\delta}_{e,ijk}\right)\left(\bar{\delta}_{e,ijk}-\omega_{e,ijk}\right)}\omega_{e,ijk}^2 \tag{29}$$

Substituting Eq. (24) and (29) into (19) gets

$$\dot{V}_1 = \sum_{i=1}^{N} m_i s_i^{\mathrm{T}}\dot{s}_i$$
$$= -k_{1,i}s_i^{\mathrm{T}}\eta_{s,i}z_{s,i} - k_{2,i}s_i^{\mathrm{T}}\sum_{j\in\mathcal{N}_i} a_{ij}\eta_{e,ij}z_{e,ij}$$
$$+\tilde{m}_i s_i^{\mathrm{T}}\varphi_i\left(p_i,p_{i,d},v_i,v_{i,d}\right) - s_i^{\mathrm{T}}u_{dr,i} + s_i^{\mathrm{T}}d_i$$
$$\le -k_{1,i}\xi_{s,i}^{*}\omega_{s,i}^{\mathrm{T}}\omega_{s,i} + \tilde{m}_i s_i^{\mathrm{T}}\varphi_i\left(p_i,p_{i,d},v_i,v_{i,d}\right)$$
$$-s_i^{\mathrm{T}}u_{dr,i} + s_i^{\mathrm{T}}d_i$$
$$-\frac{1}{2}k_{2,i}\sum_{i=1}^{N}\sum_{j\in\mathcal{N}_i}\sum_{k=1}^{3}\frac{a_{ij}\left(s_{ik}-s_{jk}\right)\xi_{e,ijk}}{\rho_{e,ij}(t)}$$
$$\times\ln\left(\frac{\underline{\delta}_{e,ijk}\bar{\delta}_{e,ijk}+\bar{\delta}_{s,ijk}\omega_{e,ijk}}{\underline{\delta}_{e,ijk}\bar{\delta}_{e,ijk}-\underline{\delta}_{e,ijk}\omega_{e,ijk}}\right)$$
$$\le -k_{1,i}\xi_{s,i}^{*}\omega_{s,i}^{\mathrm{T}}\omega_{s,i} - \frac{1}{2}k_{2,i}\sum_{i}^{N}\sum_{j\in\mathcal{N}_i} a_{ij}\xi_{e,ij}^{*}\omega_{e,ij}^{\mathrm{T}}\omega_{e,ij}$$
$$+\tilde{m}_i s_i^{\mathrm{T}}\varphi_i\left(p_i,p_{i,d},v_i,v_{i,d}\right) - s_i^{\mathrm{T}}u_{dr,i} + s_i^{\mathrm{T}}d_i \tag{30}$$

where $\xi_{s,i}^{*} = \mathrm{diag}\left\{\xi_{s,i1}^{*},\xi_{s,i2}^{*},\xi_{s,i3}^{*}\right\}$, $\xi_{e,ij}^{*} = \mathrm{diag}\left\{\xi_{e,ij1}^{*},\xi_{e,ij2}^{*},\xi_{e,ij3}^{*}\right\}$ and their k th dimensional element satisfies

$$\begin{cases}\xi_{s,ik}^{*} = \dfrac{1}{\left(\omega_{s,ik}+\underline{\delta}_{s,ik}\right)\left(\bar{\delta}_{s,ik}-\omega_{s,ik}\right)} > 0\\ \xi_{e,ijk}^{*} = \dfrac{1}{\left(\omega_{e,ijk}+\underline{\delta}_{e,ijk}\right)\left(\bar{\delta}_{e,ijk}-\omega_{e,ijk}\right)} > 0\end{cases} \tag{31}$$

To continue, choose the second Lyapunov function as:

$$V_2 = V_1 + \frac{1}{2}\sum_{i=1}^{N}\frac{1}{\kappa_{m,i}}\tilde{m}_i^2 + \frac{1}{2}\sum_{i=1}^{N}\frac{1}{\kappa_{d,i}}\tilde{d}_{i,0}^2 \tag{32}$$

where $\tilde{m}_i = m_i - \hat{m}_i$, $\tilde{d}_{i,0} = d_{i,0} - \hat{d}_{i,0}$ are the relevant estimation errors for spacecraft mass and external space perturbations. Taking the time-derivative of V_2 yields

$$\dot{V}_2 = \dot{V}_1 + \sum_{i=1}^{N}\frac{1}{\kappa_{m,i}}\tilde{m}_i\dot{\tilde{m}}_i + \sum_{i=1}^{N}\frac{1}{\kappa_{d,i}}\tilde{d}_{i,0}\dot{\tilde{d}}_{i,0} \tag{33}$$

Based on *Assumptions 1* and *2*, there are $\dot{\tilde{m}}_i = -\dot{\hat{m}}_i$, $\dot{\tilde{d}}_{i,0} = -\dot{\hat{d}}_{i,0}$. Meanwhile, according to Eq. (30), $\dot{V}_2$ satisfies:

$$\dot{V}_2 = \dot{V}_1 - \sum_{i=1}^{N}\frac{1}{\kappa_{m,i}}\tilde{m}_i\dot{\hat{m}}_i - \sum_{i=1}^{N}\sum_{k=1}^{3}\frac{1}{\kappa_{d,i}}\tilde{d}_{ik}\dot{\hat{d}}_{ik}$$
$$\le -k_{1,i}\xi_{s,i}^{*}\omega_{s,i}^{\mathrm{T}}\omega_{s,i} - \frac{1}{2}k_{2,i}\sum_{i}^{N}\sum_{j\in\mathcal{N}_i} a_{ij}\xi_{e,ij}^{*}\omega_{e,ij}^{\mathrm{T}}\omega_{e,ij}$$

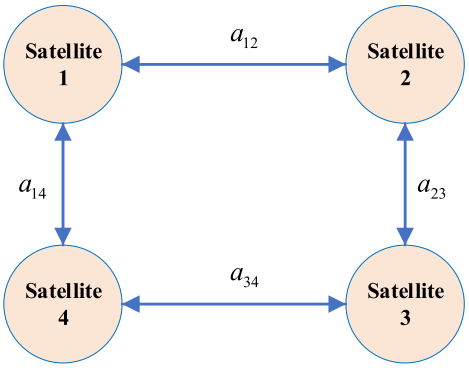

FIGURE 3. Communication topology among the four micro-satellites.

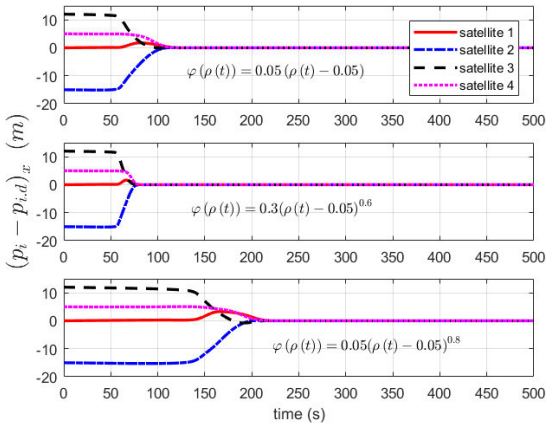

FIGURE 4. Position tracking errors of the four micro-satellites in the x-axis under the three different performance functions.

$$-\sum_{i=1}^{N}\frac{1}{\kappa_{m,i}}\tilde{m}_i\dot{\hat{m}}_i-\sum_{i=1}^{N}\sum_{k=1}^{3}\frac{1}{\kappa_{d,i}}\tilde{d}_{ik}\dot{\hat{d}}_{ik}$$
$$+\tilde{m}_i\boldsymbol{s}_i^{\mathrm{T}}\boldsymbol{\varphi}_i\left(\boldsymbol{p}_i,\boldsymbol{p}_{i,d},\boldsymbol{v}_i,\boldsymbol{v}_{i,d}\right)-\boldsymbol{s}_i^{\mathrm{T}}\boldsymbol{u}_{dr,i}+\sum_{k=1}^{3}s_{ik}d_{ik} \quad (34)$$

With consideration the detailed form of disturbance-rejection controller $\boldsymbol{u}_{dr,i}$ in Eq. (12), two cases are organized as follows.

Case 1: When $|s_{ik}| \geq \varepsilon_{i,0}$, based on Eqs. (12) and (14), Eq. (34) can be simplified as

$$\begin{aligned}\dot{V}_2 &\leq -k_{1,i}\boldsymbol{\xi}_{s,i}^{*}\boldsymbol{\omega}_{s,i}^{\mathrm{T}}\boldsymbol{\omega}_{s,i}-\frac{1}{2}k_{2,i}\sum_{i}^{N}\sum_{j\in\mathcal{N}_i}a_{ij}\boldsymbol{\xi}_{e,ij}^{*}\boldsymbol{\omega}_{e,ij}^{\mathrm{T}}\boldsymbol{\omega}_{e,ij}\\&\quad-\sum_{i=1}^{N}\tilde{d}_{i,0}\left\|\boldsymbol{s}_i\right\|_1+\sum_{i=1}^{N}\sum_{k=1}^{3}s_{ik}\left(d_{i,0}-\frac{s_{ik}}{|s_{ik}|}\hat{d}_{i,0}\right)\\&\leq -k_{1,i}\boldsymbol{\xi}_{s,i}^{*}\boldsymbol{\omega}_{s,i}^{\mathrm{T}}\boldsymbol{\omega}_{s,i}-\frac{1}{2}k_{2,i}\sum_{i}^{N}\sum_{j\in\mathcal{N}_i}a_{ij}\boldsymbol{\xi}_{e,ij}^{*}\boldsymbol{\omega}_{e,ij}^{\mathrm{T}}\boldsymbol{\omega}_{e,ij}\\&\quad-\sum_{i=1}^{N}\tilde{d}_{i,0}\left\|\boldsymbol{s}_i\right\|_1+\sum_{i=1}^{N}\left(d_{i,0}-\hat{d}_{i,0}\right)\left\|\boldsymbol{s}_i\right\|_1\\&\leq -k_{1,i}\boldsymbol{\xi}_{s,i}^{*}\boldsymbol{\omega}_{s,i}^{\mathrm{T}}\boldsymbol{\omega}_{s,i}-\frac{1}{2}k_{2,i}\sum_{i}^{N}\sum_{j\in\mathcal{N}_i}a_{ij}\boldsymbol{\xi}_{e,ij}^{*}\boldsymbol{\omega}_{e,ij}^{\mathrm{T}}\boldsymbol{\omega}_{e,ij} \quad (35)\end{aligned}$$

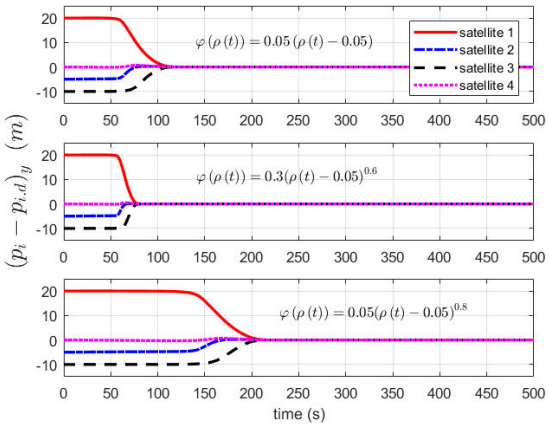

FIGURE 5. Position tracking errors of the four micro-satellites in the y-axis under the three different performance functions.

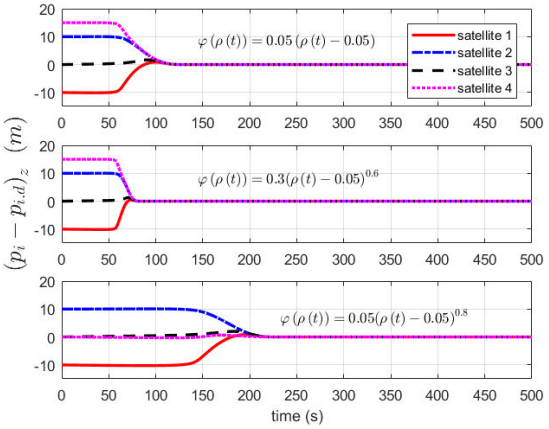

FIGURE 6. Position tracking errors of the four micro-satellites in the z-axis under the three different performance functions.

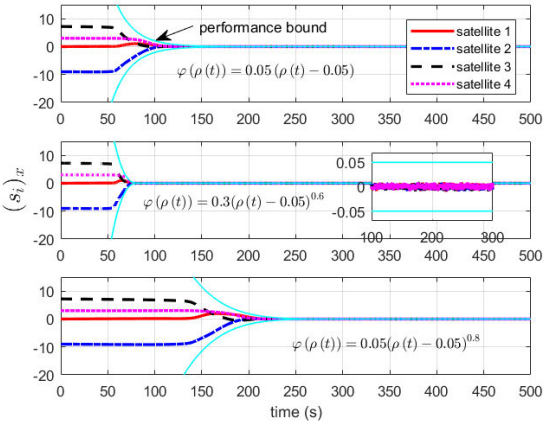

FIGURE 7. Time responses of the intermediate variable for the four micro-satellites in the x-axis with guaranteed performance.

Based on the above equation, it is easy to find that the tracking errors of the SFF system are convergent under the devised adaptive coordinated controller. Namely, the prescribed performance envelope can be achieved.

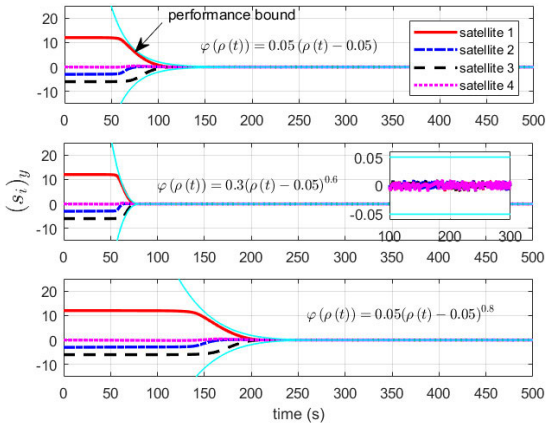

FIGURE 8. Time responses of the intermediate variable for the four micro-satellites in the y-axis with guaranteed performance.

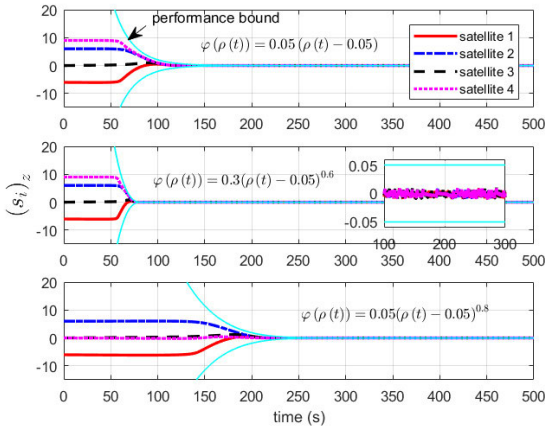

FIGURE 9. Time responses of the intermediate variable for the four micro-satellites in the z-axis with guaranteed performance.

Case 2: When $|s_{ik}| < \varepsilon_{i,0}$, based on Eqs. (12) and (14), Eq. (34) can be simplified as

$$\begin{aligned}
\dot{V}_2 \leq & -k_{1,i}\boldsymbol{\xi}_{s,i}^{*}\boldsymbol{\omega}_{s,i}^{\mathrm{T}}\boldsymbol{\omega}_{s,i} - \frac{1}{2}k_{2,i}\sum_{i}^{N}\sum_{j\in\mathcal{N}_i} a_{ij}\boldsymbol{\xi}_{e,ij}^{*}\boldsymbol{\omega}_{e,ij}^{\mathrm{T}}\boldsymbol{\omega}_{e,ij} \\
& - \sum_{i=1}^{N}\tilde{d}_{i,0}\left\|\boldsymbol{s}_i\right\|_1 - \sum_{i=1}^{N}\sum_{k=1}^{3}\frac{s_{ik}^2\hat{d}_{i,0}^2}{\varepsilon_{i,0}^2} + \sum_{i=1}^{N}\sum_{k=1}^{3}s_{ik}d_{i,0} \\
\leq & -k_{1,i}\boldsymbol{\xi}_{s,i}^{*}\boldsymbol{\omega}_{s,i}^{\mathrm{T}}\boldsymbol{\omega}_{s,i} - \frac{1}{2}k_{2,i}\sum_{i}^{N}\sum_{j\in\mathcal{N}_i} a_{ij}\boldsymbol{\xi}_{e,ij}^{*}\boldsymbol{\omega}_{e,ij}^{\mathrm{T}}\boldsymbol{\omega}_{e,ij} \\
& - \sum_{i=1}^{N}\sum_{k=1}^{3}\frac{s_{ik}^2\hat{d}_{i,0}^2}{\varepsilon_{i,0}^2} + \sum_{i=1}^{N}\left\|\boldsymbol{s}_i\right\|_1\hat{d}_{i,0} \\
\leq & -k_{1,i}\boldsymbol{\xi}_{s,i}^{*}\boldsymbol{\omega}_{s,i}^{\mathrm{T}}\boldsymbol{\omega}_{s,i} - \frac{1}{2}k_{2,i}\sum_{i}^{N}\sum_{j\in\mathcal{N}_i} a_{ij}\boldsymbol{\xi}_{e,ij}^{*}\boldsymbol{\omega}_{e,ij}^{\mathrm{T}}\boldsymbol{\omega}_{e,ij} \\
& - \sum_{i=1}^{N}\sum_{k=1}^{3}\left(\frac{|s_{ik}|\,\hat{d}_{i,0}}{\varepsilon_{i,0}} - \frac{1}{2}\varepsilon_{i,0}\right)^2 + \frac{1}{4}\sum_{i=1}^{N}\varepsilon_{i,0}^2 \qquad (36)
\end{aligned}$$

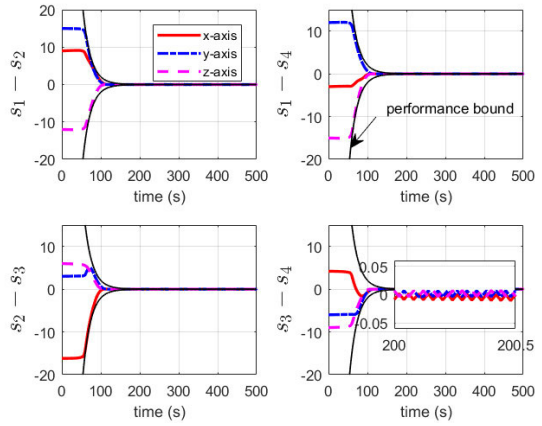

FIGURE 10. Time responses of the consensus errors $(s_i - s_j)$ for the four micro-satellites with guaranteed performance under the performance function derived by $\mathcal{K}_\infty$-type function $0.05\ (\rho_i(t) - 0.05)$.

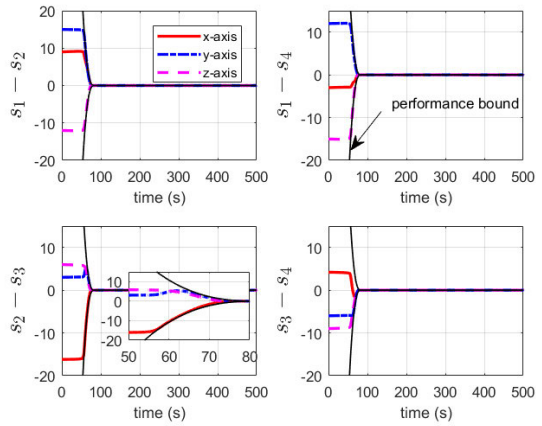

FIGURE 11. Time responses of the consensus errors $(s_i - s_j)$ for the four micro-satellites with guaranteed performance under the performance function derived by $\mathcal{K}_\infty$-type function $0.3(r_i(t) - 0.05)^{0.6}$.

As presented in Eq. (36), it is easy to find that the tracking errors are convergent to a small neighbourhood around zero. Namely, the predefined performance envelope can be guaranteed under the adjustable performance function and all the close-loop signals are uniformly ultimately bounded.

Based on the stability analysis in *Cases 1* and *2*, the proof of *Theorem 1* is completed. ■

Remark 5: As shown in Eq. (31), when $\omega_{s,ik} \to -\underline{\delta}_{s,ik}$ or $\omega_{s,ik} \to \bar{\delta}_{s,ik}$, parameter $\boldsymbol{\xi}_{s,ik}^{*}$ will become very large. Similarly, when $\omega_{e,ijk} \to -\underline{\delta}_{e,ijk}$ or $\omega_{e,ijk} \to \bar{\delta}_{e,ijk}$, parameter $\boldsymbol{\xi}_{s,ik}^{*}$ will also become very large. In this case, the absolute values of parameters $-k_{1,i}\boldsymbol{\xi}_{s,i}^{*}$ and $-0.5k_{2,i}\boldsymbol{\xi}_{e,ij}^{*}$, convergence rate indicators for variables $\omega_{s,ik}$, will become very large. This implies that when the tracking errors of the SFF system converge to the performance bound, there exist large control forces steering the tracking error system to run in the opposite direction. When $\omega_{s,ik} \to 0$ or $\omega_{e,ijk} \to 0$, parameters $\boldsymbol{\xi}_{s,ik}^{*}$ and $\boldsymbol{\xi}_{e,ijk}^{*}$ will become very small. In this sense, the absolute values of the convergence indicators $-k_{1,i}\boldsymbol{\xi}_{s,i}^{*}$ and

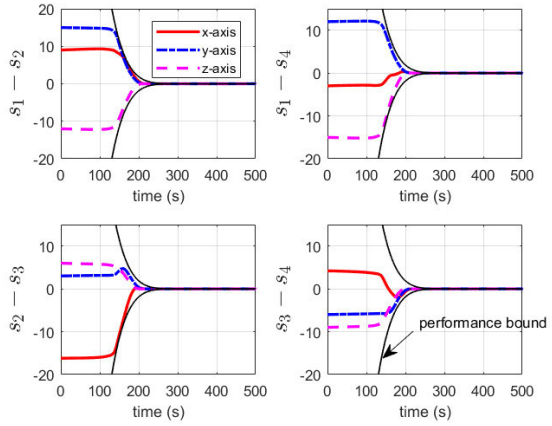

FIGURE 12. Time responses of the consensus errors $(s_i - s_j)$ for the four micro-satellites with guaranteed performance under the performance function derived by $\mathcal{K}_\infty$-type function $0.05(\rho_i(t) - 0.05)^{0.8}$.

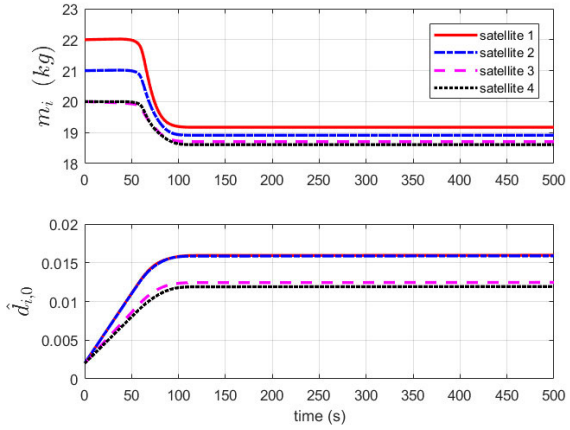

FIGURE 13. Time responses of the adaptive parameters $\hat{m}_i$, $\hat{d_{i,0}}$ under the performance function derived by $\mathcal{K}_\infty$-type function $0.05(\rho_i(t) - 0.05)$.

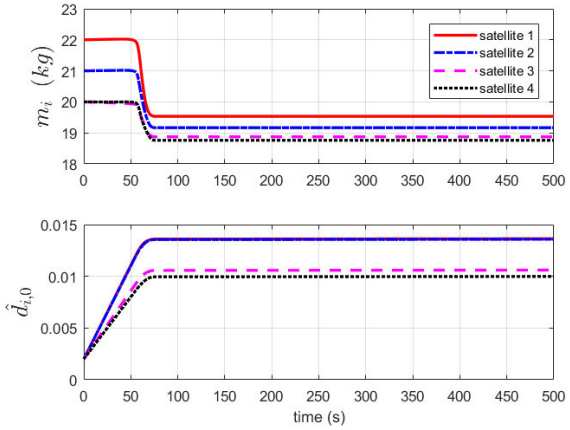

FIGURE 14. Time responses of the adaptive parameters $\hat{m}_i$, $\hat{d_{i,0}}$ under the performance function derived by $\mathcal{K}_\infty$-type function $0.3(\rho_i(t) - 0.05)^{0.6}$.

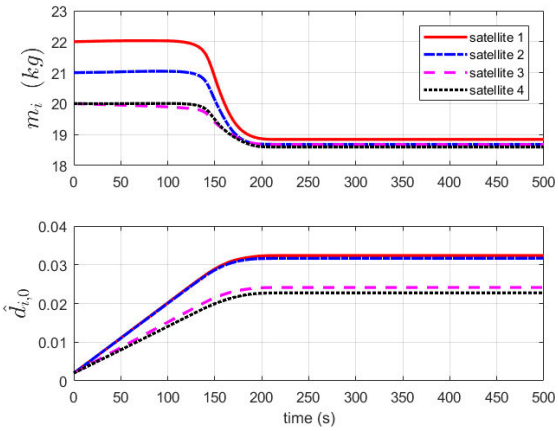

FIGURE 15. Time responses of the adaptive parameters $\hat{m}_i$, $\hat{d_{i,0}}$ under the performance function derived by $\mathcal{K}_\infty$-type function $0.05(\rho_i(t) - 0.05)^{0.8}$.

TABLE 1. Simulation parameters.

Parameters	Values
Orbital parameters	a_c=7000 km, $e_c = 0.02, \theta_c(0) = 0$ rad
	$\gamma_i = \text{diag}\{0.6, 0.6, 0.6\}$, $k_{1,i} = 5$, $k_{2,i} = 3$
Controller parameters	$\varepsilon_{i,0} = 0.005$, $\hat{d}_{i,0}(0) = 0.002$, $\hat{m}_1(0) = 22$
	$\hat{m}_2(0) = 21$, $\hat{m}_3(0) = 20$, $\hat{m}_4(0) = 20$
	$\kappa_{m,i} = 1/30$, $\kappa_{d,i} = 10^{-5}$, $I_{i,sp} = 200\ (i = 1,2,3,4)$
Initial conditions	$\boldsymbol{p}_1(0) = [250, 20, 423]^{\mathrm{T}}$ m
	$\boldsymbol{p}_2(0) = [-15, -505, 10]^{\mathrm{T}}$ m
	$\boldsymbol{p}_3(0) = [-238, -10, -250\sqrt{3}]^{\mathrm{T}}$ m
	$\boldsymbol{p}_2(0) = [5, 500, 15]^{\mathrm{T}}$ m
	$\boldsymbol{v}_i = [0, 0, 0]^{\mathrm{T}}$ m/s $(i = 1,2,3,4)$
Desired conditions	$\boldsymbol{p}_{0,d} = (1 - \exp(-0.5t/\Gamma))[300, 0, 0]^{\mathrm{T}}$ m
	$\boldsymbol{p}_{i,f} = \tilde{\lambda}(t)\mathcal{R}(\hbar(t))\bar{\boldsymbol{p}}_{i,f}$
	$\Gamma = -0.04(2\pi/\omega_c)^2/(2\ln 10^{-6})$
	$\tilde{\lambda}(t) = 1 + 3(1 - \exp(-0.5t/\Gamma))/5$
	$\hbar(t) = \pi(1 - \exp(-0.5t/\Gamma))/6$
	$\mathcal{R}(\hbar(t)) = [\cos(\hbar(t)), 0, -\sin(\hbar(t)); 0, 1, 0;$
	$\sin(\hbar(t)), 0, \cos(\hbar(t))]$
	$\bar{\boldsymbol{p}}_{i,f} = 500[1/2\cos(\phi_i), -\sin(\phi_i),$
	$\sqrt{3}/2\cos(\phi_i)]$
	$\phi_1 = 0, \phi_2 = \pi/2, \phi_3 = \pi, \phi_4 = 3\pi/2$

$-0.5k_{2,i}\boldsymbol{\xi}^*_{e,ij}$ will be very small. Namely, when the tracking errors are very small, the relevant control forces are very small to guarantee the predefined performance. Based on the aforementioned discussions and analysis, the convergence performance of the proposed control approach is adjustable

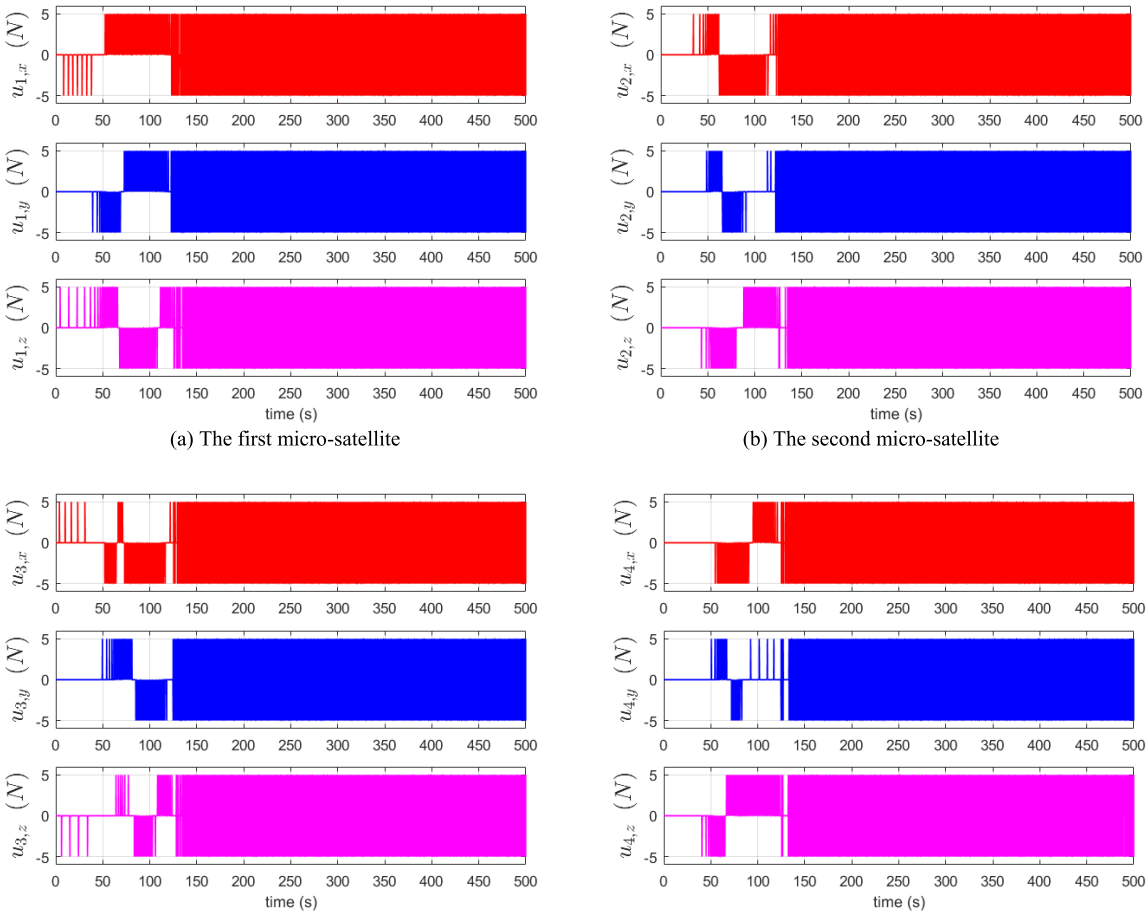

(a) The first micro-satellite (b) The second micro-satellite

(c) The third micro-satellite (d) The fourth micro-satellite

FIGURE 16. Control forces governed by the PWPF technique of the four micro-satellites under the performance function derived by $\mathcal{K}_\infty$-type function $0.05(\rho_i(t) - 0.05)$.

by two ways: on one hand, the different choice of the $\mathcal{K}_\infty$-type function will determine the transient and steady-state performance of function $\rho(t)$. This will influence the convergence of the tracking errors of the SFF system. On the other hand, the ingenious configuration of adaptive coordinated controller in Eq. (12) leads two convergence indicators $\boldsymbol{\xi}^*_{s,ik}, \boldsymbol{\xi}^*_{e,ijk}$ in Eq. (31) which change with the tracking errors. This in turn adjusts the convergence rate adaptively and indirectly. Thus, the tracking performance under the devised controller is adjustable and can be configured by the users.

Remark 6: In practice, with consideration of the force saturation, the convergence rate of the adjustable performance function will be limited. In this case, some desired transient performance cannot be achieved. This is the conservatism of the proposed coordinated control approach. To solve this problem, the relevant parameters of the performance functions can be set by the maximal forces of the thrusts in practical engineering tasks. Commonly, if the output of the thrusts is large, then the convergence rate of the adjustable performance function can be set as a large value and vice versa.

Remark 7: As presented in Eq. (14), the adaptive parameters $\hat{m}_i, \hat{d}_{i,0}$ will be sensitive to the filtered state variable $\boldsymbol{s}_i$, which leads to a high computation burden. To avoid such problem, inspired by Ref. [41], an artificial dead-zone operator can be applied to replace Eq. (14), which is expressed by

$$\begin{cases} \dot{\hat{m}}_i = \begin{cases} \kappa_{m,i}\boldsymbol{s}_i^{\mathrm{T}}\boldsymbol{\varphi}_i\left(\boldsymbol{p}_i, \boldsymbol{p}_{i,d}, \boldsymbol{v}_i, \boldsymbol{v}_{i,d}\right), & \|\boldsymbol{s}_i\| > \Omega_{i,0} \\ 0, & \text{otherwise} \end{cases} \\ \dot{\hat{d}}_{i,0} = \begin{cases} \kappa_{d,i}\|\boldsymbol{s}_i\|_1, & \|\boldsymbol{s}_i\| > \Omega_{i,0} \\ 0, & \text{otherwise} \end{cases} \end{cases} \tag{37}$$

where $\Omega_{i,0}$ is a small positive constant.

IV. ILLUSTRATIVE EXAMPLES

To verify the performance of the proposed adaptive coordinated control approach, a group of numerical examples are organized in this section. Consider that there are four micro-satellites in the SFF system, which formulates a specific square configuration for some deep-space observation missions. To achieve a high image resolution and improve the

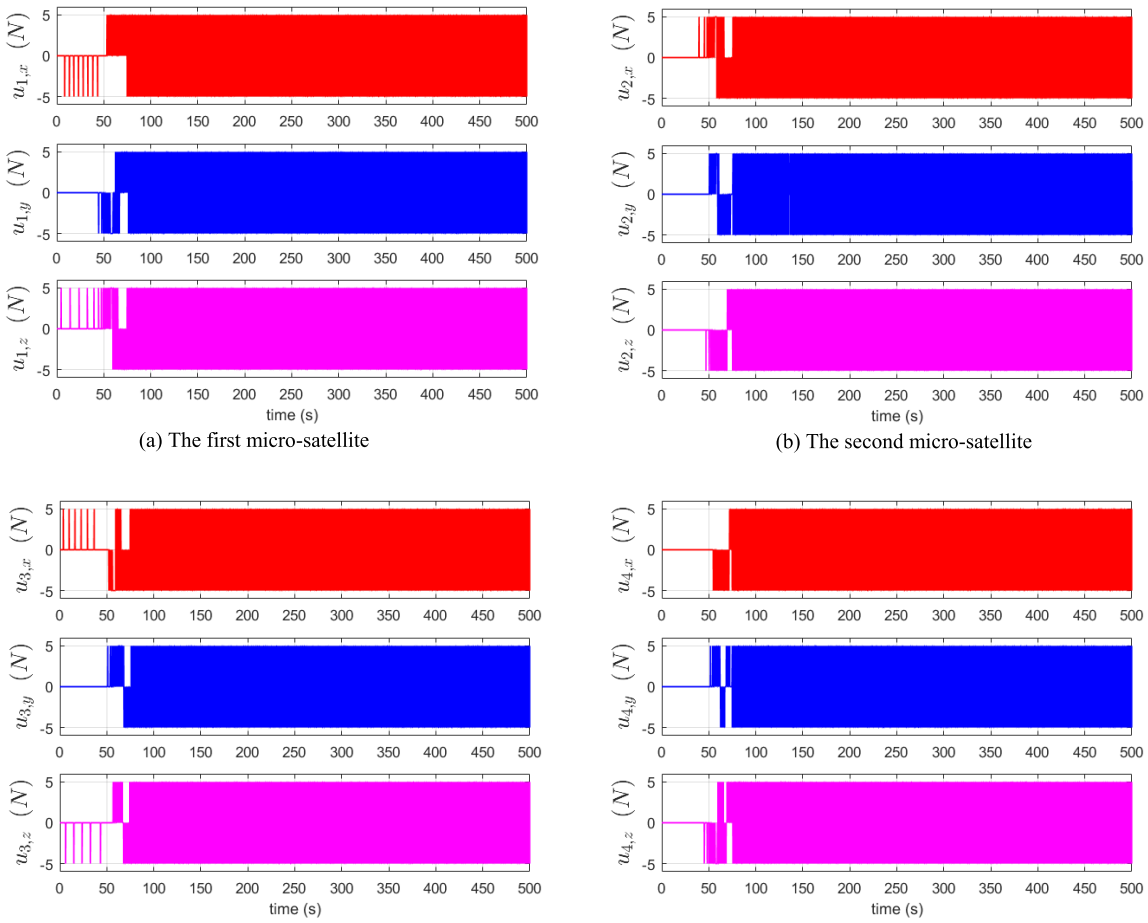

(a) The first micro-satellite

(b) The second micro-satellite

(c) The third micro-satellite

(d) The fourth micro-satellite

FIGURE 17. Control forces governed by the PWPF technique of the four micro-satellites under the performance function derived by $\mathcal{K}_\infty$-type function $0.05(\rho_i(t) - 0.05)$.

image quality, the size of the formation geometry is required to increase [40]. Thereby, the SFF system is expected to carry out a desired formation maneuver while preserving the scheduled formation configuration intact during the orbital maneuvers. The communication topology among the four micro-satellites is illustrated in Fig. 3. It is assumed that the nominal masses of the four micro-satellites are 20 kg. With consideration of fuel consumptions of the thruster equipped on the micro-satellites, the mass flow of each micro-satellite is given by [42]

$$\dot{m}_i = -\sum_{j=1}^{3} \left|u_{i,j}\right| / \left(I_{i,sp} g\right) \tag{38}$$

where $g = \mu / R_i^2$ is the gravitational constant. $I_{i,sp}$ denotes the specific impulse. $u_{i,j}$ is the j th dimensional element of the control force $\boldsymbol{u}_i$. To test the robustness of the proposed coordinated control approach, it is assumed that the space perturbations $\boldsymbol{d}_i$ are uniformly selected as $0.001\,[\sin(t/10), \cos(t/15), \sin(t/20)]^{\mathrm{T}}$ N. To demonstrate the adjustable performance of the performance function, we organize the relevant numerical simulations under three different performance functions. Without loss of generality, all the performance functions for each spacecraft in the SFF system are the same and the relevant parameters $\underline{\delta}_{s,ik}, \bar{\delta}_{s,ik}, \underline{\delta}_{e,ijk}, \bar{\delta}_{e,ijk}$ in the performance functions are set as $\underline{\delta}_{s,ik} = \bar{\delta}_{s,ik} = \underline{\delta}_{e,ijk} = \bar{\delta}_{e,ijk} = 1\,(i = 1, 2, 3, 4, j = 1, 2, 3, k = 1, 2, 3)$. Moreover, the three performance functions mentioned above are derived by three $\mathcal{K}_\infty$-type functions $\varphi_i(\rho_i(t))$, i.e., $0.05(\rho_i(t) - 0.05)$, $0.05(\rho_i(t) - 0.05)^{0.8}$, $0.3\left(\rho_i(t) - 0.05\right)^{0.6}$, respectively $(i = 1, 2, 3, 4)$. In this sense, the steady-state performance bound is 0.05. Namely, the upper bounds of the tracking errors 0.05. With consideration of the thrusters equipped on all the microsatellites, the control signals computed by the proposed control approach should be modulated to pulse trains by applying the PWPF technique with the saturation bound of the thrusters being set as 5 N. Wherein, the detailed introduction of the PWPF technique can be referred to Ref. [43], which is omitted for brevity. The simulation parameters and state conditions are presented in Table 1. Accordingly, the corresponding simulation results are presented in Figs. 4 to 19.

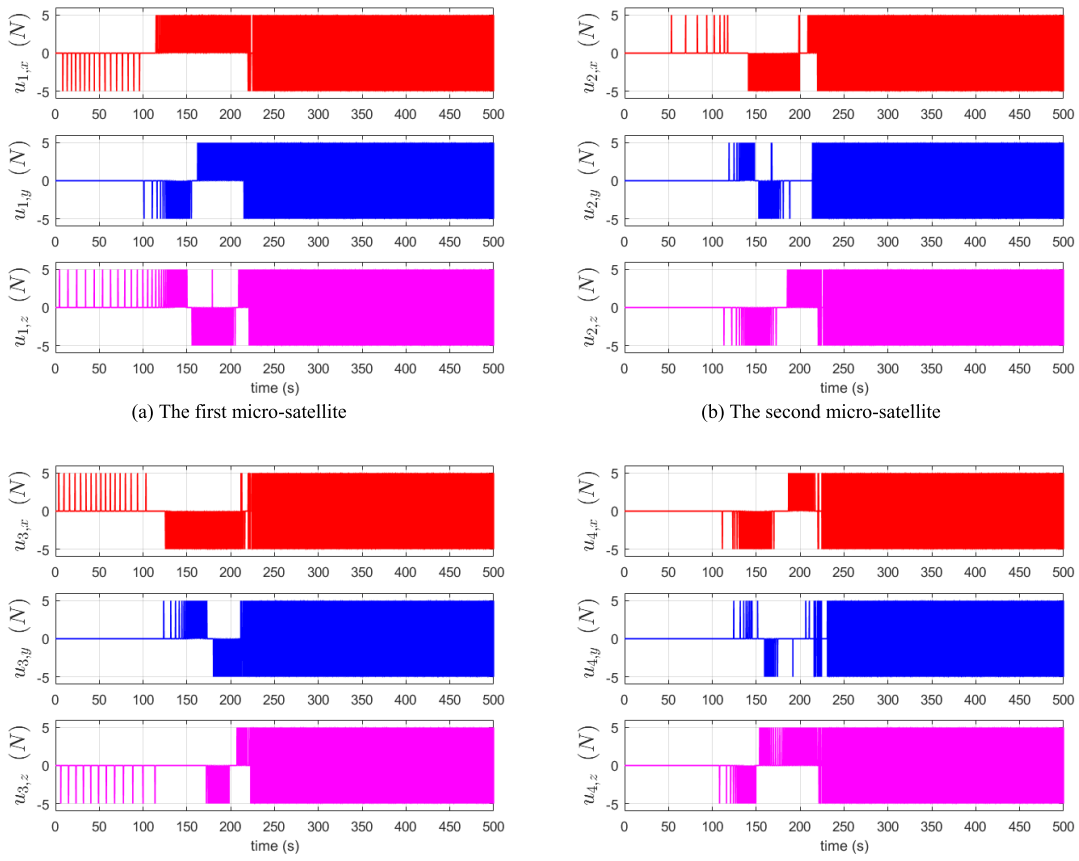

(a) The first micro-satellite

(b) The second micro-satellite

(c) The third micro-satellite

(d) The fourth micro-satellite

FIGURE 18. Control forces governed by the PWPF technique of the four micro-satellites under the performance function derived by $\mathcal{K}_\infty$-type function $0.05(\rho_i(t) - 0.05)$.

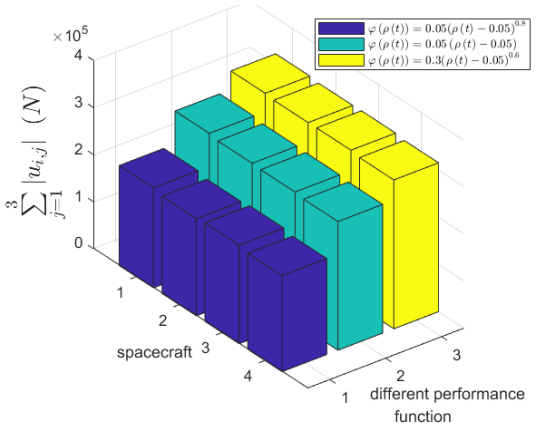

FIGURE 19. Comparisons on the fuel consumptions of the four micro-satellites under the three performance functions.

As presented in Figs. 4 to 19, one can conclude that: 1) Figs. 4 to 6 demonstrate the time responses of the position tracking errors of the four micro-satellites under the three different performance functions. From the simulation results, it is easy to find that the convergence rates of position tracking errors are different. Namely, the convergence time is 120 s, 70 s and 200 s for the $\mathcal{K}_\infty$-type functions $0.05\,(\rho_i\,(t) - 0.05)$, $0.3\,(\rho_i\,(t) - 0.05)^{0.6}$ and $0.05\,(\rho_i\,(t) - 0.05)^{0.8}$ respectively. From the convergence time for the three $\mathcal{K}_\infty$-type functions, one can find that the larger the proportional parameters of the $\mathcal{K}_\infty$-type functions are, the faster the convergence rate is. Figs. 7 to 9 illustrate the time responses of the intermediate variable $\boldsymbol{s}_i$ for the four micro-satellites under the three $\mathcal{K}_\infty$-type functions. It is obvious that all the trajectories of the variable $\boldsymbol{s}_i$ are involved in the predefined performance envelopes. Similarly, the transient and steady-state consensus performance for the tracking errors $(\boldsymbol{s}_i - \boldsymbol{s}_j)$ of the four micro-satellites is also preserved in the whole time domain as illustrated in Figs. 10 to 12. To be brief, the simulations in Figs. 4 to 12 imply that the desired position commands can be tracked under the devised adaptive coordinated controller with preserving the scheduled formation configuration intact. Moreover, the time responses of the adaptive parameters $\hat{m}_i$, $\hat{d}_{i,0}$ for the four micro-satellites are given in Figs. 13 to 15. Under the devised adaptive schemes, the adaptive parameters mentioned above are convergent. Thus, the adaptive schemes are effective. Figs. 16 to 19 present the control forces of the four micro-satellites under the three different performance functions. From the simulation results, one can

find that the control input does not validate the saturation bounds under the PWPF technique. Meanwhile, it requires large fuel consumptions when the $\mathcal{K}_\infty$-type function induces fast convergence rate of the position tracking error system of the micro-satellite.

To sum up, the simulation results in this part demonstrate the effectiveness of the proposed adaptive coordinated control approach for the SFF system.

V. CONCLUSION

In this paper, an adaptive coordinated control approach for the spacecraft formation flying has been developed with guaranteed tracking performance and preservation for the scheduled formation configuration intact. Compared with the existing coordinated control approaches, the major difference is that the transient and steady-state performance of the position tracking errors and consensus errors are guaranteed under the devised controller. Moreover, a general unified form of the adjustable performance function is established based on which the convergence and tracking error bound can be configured freely by the users. Wherein, the existing exponentially and finite-time convergent performance functions can be expressed by the proposed general unified form. The corresponding simulation results demonstrate the effectiveness of the proposed coordinated control approach in preserving the adjustable tracking performance and scheduled formation configuration impact for the SFF system.

REFERENCES

[1] W. Ren and R. W. Beard, "Decentralized scheme for spacecraft formation flying via the virtual structure approach," *J. Guid., Control, Dyn.*, vol. 27, no. 1, pp. 73–82, 2004.

[2] R. Liu, X. Cao, and M. Liu, "Finite-time synchronization control of spacecraft formation with network-induced communication delay," *IEEE Access*, vol. 5, pp. 27242–27253, 2017.

[3] C. Zhang, M. Z. Dai, J. Wu, B. Xiao, B. Li, and M. Wang, "Neural-networks and event-based fault-tolerant control for spacecraft attitude stabilization," *Aerosp. Sci. Technol.*, vol. 114, Jul. 2021, Art. no. 106746.

[4] M. G. Di, M. Lawn, and R. Bevilacqua, "Survey on guidance navigation and control requirements for spacecraft formation-flying missions," *J. Guid. Control Dyn.*, vol. 41, no. 3, pp. 581–602, 2018.

[5] R. Kristiansen and P. J. Nicklasson, "Spacecraft formation flying: A review and new results on state feedback control," *Acta Astronaut.*, vol. 65, nos. 11–12, pp. 1537–1552, 2009.

[6] L. Chen, C. Li, Y. Guo, G. Ma, and B. Zhu, "Spacecraft formation-containment flying control with time-varying translational velocity," *Chin. J. Aeronaut.*, vol. 33, no. 1, pp. 271–281, 2020.

[7] D. Lee, A. K. Sanyal, and E. A. Butcher, "Asymptotic tracking control for spacecraft formation flying with decentralized collision avoidance," *J. Guid., Control, Dyn.*, vol. 38, no. 4, pp. 587–600, Apr. 2015.

[8] R. Schlanbusch, R. Kristiansen, and P. J. Nicklasson, "Spacecraft formation reconfiguration with collision avoidance," *Automatica*, vol. 47, no. 7, pp. 1443–1449, Jul. 2011.

[9] W. Wang, C. Li, and Y. Guo, "Relative position coordinated control for spacecraft formation flying with obstacle/collision avoidance," *Nonlinear Dyn.*, vol. 104, no. 2, pp. 1329–1342, Apr. 2021, doi: 10.1007/s11071-021-06348-9.

[10] D. Ran, X. Chen, A. K. Misra, and B. Xiao, "Relative position coordinated control for spacecraft formation flying with communication delays," *Acta Astronaut.*, vol. 137, pp. 302–311, Aug. 2017.

[11] J. Bae and Y. Kim, "Adaptive controller design for spacecraft formation flying using sliding mode controller and neural networks," *J. Franklin Inst.*, vol. 349, no. 2, pp. 578–603, Mar. 2012.

[12] J. Sun, X. Zhao, J. Fang, and Y. Wang, "Autonomous memristor chaotic systems of infinite chaotic attractors and circuitry realization," *Nonlinear Dyn.*, vol. 94, no. 4, pp. 2879–2887, 2018.

[13] J. Sun, Y. Wu, G. Cui, and Y. Wang, "Finite-time real combination synchronization of three complex-variable chaotic systems with unknown parameters via sliding mode control," *Nonlinear Dyn.*, vol. 88, no. 3, pp. 1677–1690, 2017.

[14] S. J. Chung, U. Ahsun, and J. J. E. Slotine, "Application of synchronization to formation flying spacecraft: Lagrangian approach," *J. Guid. Control Dynam.*, vol. 32, no. 2, pp. 512–526, 2009.

[15] H. Sun, S. Li, and S. Fei, "A composite control scheme for 6DOF spacecraft formation control," *Acta Astron.*, vol. 69, nos. 7–8, pp. 595–611, 2011.

[16] Q. Hu and J. Zhang, "Relative position finite-time coordinated tracking control of spacecraft formation without velocity measurements," *ISA Trans.*, vol. 54, pp. 60–74, Jan. 2015.

[17] M. Zhuang, L. Tan, K. Li, and S. Song, "Fixed-time position coordinated tracking control for spacecraft formation flying with collision avoidance," *Chin. J. Aeronaut.*, to be published, doi: 10.1016/j.cja.2020.12.024.

[18] W. Zou, P. Shi, Z. Xiang, and Y. Shi, "Finite-time consensus of second-order switched nonlinear multi-agent systems," *IEEE Trans. Neural Netw. Learn. Syst.*, vol. 31, no. 5, pp. 1757–1762, Jun. 2019.

[19] C. P. Bechlioulis and G. A. Rovithakis, "Robust adaptive control of feedback linearizable MIMO nonlinear systems with prescribed performance," *IEEE Trans. Automat. Control*, vol. 53, no. 9, pp. 2090–2099, Oct. 2008.

[20] X. Bu, Y. Xiao, and H. Lei, "An adaptive critic design-based fuzzy neural controller for hypersonic vehicles: Predefined behavioral nonaffine control," *IEEE/ASME Trans. Mechatron.*, vol. 24, no. 4, pp. 1871–1881, Jul. 2019.

[21] J. Na, Q. Chen, X. Ren, and Y. Guo, "Adaptive prescribed performance motion control of servo mechanisms with friction compensation," *IEEE Trans. Ind. Electron.*, vol. 61, no. 1, pp. 486–494, Jan. 2013.

[22] J. X. Zhang and G. H. Yang, "Prescribed performance fault-tolerant control of uncertain nonlinear systems with unknown control directions," *IEEE Trans. Automat. Control*, vol. 62, no. 12, pp. 6529–6535, May 2017.

[23] H. Qin, Z. Wu, Y. Sun, C. Zhang, and C. Lin, "Fault-tolerant prescribed performance control algorithm for underwater acoustic sensor network nodes with thruster saturation," *IEEE Access*, vol. 7, pp. 69504–69515, 2019.

[24] Y. Shi, X. Shao, W. Yang, and W. Zhang, "Event-triggered output feedback control for MEMS gyroscope with prescribed performance," *IEEE Access*, vol. 8, pp. 26293–26303, 2020.

[25] X. Huang and G. Duan, "Fault-tolerant attitude tracking control of combined spacecraft with reaction wheels under prescribed performance," *ISA Trans.*, vol. 98, pp. 161–172, Mar. 2020.

[26] C. Wei, J. Luo, H. Dai, and G. Duan, "Learning-based adaptive attitude control of spacecraft formation with guaranteed prescribed performance," *IEEE Trans. Cybern.*, vol. 49, no. 11, pp. 4004–4016, Aug. 2019.

[27] K. Xia and Y. Zou, "Neuroadaptive saturated control for relative motion based noncooperative spacecraft proximity with prescribed performance," *Acta Astronaut.*, vol. 180, pp. 361–369, Mar. 2021.

[28] S. He, M. Wang, S. L. Dai, and F. Luo, "Leader-follower formation control of USVs with prescribed performance and collision avoidance," *IEEE Trans. Ind. Informat.*, vol. 15, no. 1, pp. 572–581, May 2018.

[29] C. Hua, J. Chen, and Y. Li, "Leader-follower finite-time formation control of multiple quadrotors with prescribed performance," *Int. J. Syst. Sci.*, vol. 48, no. 12, pp. 2499–2508, 2017.

[30] K. Sun, J. Qiu, H. R. Karimi, and Y. Fu, "Event-triggered robust fuzzy adaptive finite-time control of nonlinear systems with prescribed performance," *IEEE Trans. Fuzzy Syst.*, vol. 29, no. 6, pp. 1460–1471, Jun. 2021, doi: 10.1109/TFUZZ.2020.2979129.

[31] C. Wei, J. Luo, Z. Yin, and J. Yuan, "Leader-following consensus of second-order multi-agent systems with arbitrarily appointed-time prescribed performance," *IET Control Theory Appl.*, vol. 12, no. 16, pp. 2276–2286, 2018.

[32] Z. Yin, A. Suleman, J. Luo, and C. Wei, "Appointed-time prescribed performance attitude tracking control via double performance functions," *Aerosp. Sci. Technol.*, vol. 93, Oct. 2019, Art. no. 105337.

[33] X. Shao, Y. Shi, and W. Zhang, "Fault-tolerant quantized control for flexible air-breathing hypersonic vehicles with appointed-time tracking performances," *IEEE Trans. Aerosp. Electron. Syst.*, vol. 57, no. 2, pp. 1261–1273, Apr. 2021.

[34] W. Zou, P. Shi, Z. Xiang, and Y. Shi, "Consensus tracking control of switched stochastic nonlinear multiagent systems via event-triggered strategy," *IEEE Trans. Neural Netw. Learn. Syst.*, vol. 31, no. 3, pp. 1036–1045, Mar. 2020.
[35] X. Bu and Q. Qi, "Fuzzy optimal tracking control of hypersonic flight vehicles via single-network adaptive critic design," *IEEE Trans. Fuzzy Syst.*, early access, Nov. 11, 2020, doi: 10.1109/TFUZZ.2020.3036706.
[36] W. B. Xie, T. Z. Wang, J. Zhang, and Y. L. Wang, "H_∞ reduced-order observer-based controller synthesis approach for TS fuzzy systems," *J. Franklin Inst.*, vol. 356, no. 12, pp. 6388–6400, 2019.
[37] W. Xie, B. Liu, L. Bu, Y. Wang, and J. Zhang, "A decoupling approach for observer-based controller design of T–S fuzzy system with unknown premise variables," *IEEE Trans. Fuzzy Syst.*, early access, Jul. 2, 2020, doi: 10.1109/TFUZZ.2020.3006572.
[38] S. Xiao, X. Zhang, X. Wang, and Y. Wang, "A reduced-order approach to analyze stability of genetic regulatory networks with discrete time delays," *Neurocomputing*, vol. 323, pp. 311–318, Jan. 2019.
[39] C. Liu, X. Wang, and Y. Xue, "Global exponential stability analysis of discrete-time genetic regulatory networks with time-varying discrete delays and unbounded distributed delays," *Neurocomputing*, vol. 372, pp. 100–108, 2020.
[40] Q. Hu, Y. Shi, and C. Wang, "Event-based formation coordinated control for multiple spacecraft under communication constraints," *IEEE Trans. Syst., Man, Cybern., Syst.*, vol. 51, no. 5, pp. 3168–3179, May 2021.
[41] C. Wei, J. Luo, B. Gong, M. Wang, and J. Yuan, "On novel adaptive saturated deployment control of tethered satellite system with guaranteed output tracking prescribed performance," *Aerosp. Sci. Technol.*, vol. 75, pp. 58–73, Apr. 2018.
[42] Y. Xu, A. Tatasch, and N. Fitz-Coy, "Chattering free sliding mode control for a 6 DOF formation flying mission," in *Proc. AIAA Guid., Navigat., Control Conf. Exhib.*, Aug. 2005, pp. 6464.
[43] B. Cong, X. Liu, and Z. Chen, "A precise and robust control strategy for rigid spacecraft eigenaxis rotation," *Chin. J. Aeronaut.*, vol. 24, no. 4, pp. 484–492, 2011.

DANGJUN ZHAO received the B.S. degree in mechano-electronic engineering from Xidian University, Xi'an, China, in 2002, the M.S. degree in electronic engineering from the Wuhan Institute of Technology, Wuhan, China, in 2008, and the Ph.D. degree in control science and engineering from the Huazhong University of Science and Technology, Wuhan, in 2011.

He is currently an Associate Professor with the School of Aeronautics and Astronautics, Central South University, Changsha, China. He has authored or coauthored one book and more than 20 articles. His research interests include signal processing, and guidance and control for spacecraft.

KAI JIN received the B.S. and Ph.D. degrees from the School of Astronautics, Northwestern Polytechnical University, Xi'an, China, in 2012 and 2019, respectively.

From October 2016 to October 2018, he worked as a Visiting Ph.D. Student with the Department of Mechanical Engineering, Utah State University, Logan, UT, USA. He is currently an Engineer with the Research Institute, CETC. His research interests include prescribed performance control, trajectory optimization, and uncertainty analysis.

CAISHENG WEI received the B.S. and Ph.D. degrees from the School of Astronautics, Northwestern Polytechnical University, Xi'an, China, in 2014 and 2019, respectively.

He is currently a Professor with Central South University, Changsha, China. His research interests include prescribed performance control, learning-based adaptive control with application to spacecraft, and space robot.

Prof. Wei was a recipient of the Youth Talent Promotion of China Association for Science and Technology. He serves as the Youth Editor for *Journal of Central South University (Science and Technology)* and a Section Topics Board Editor for *Sensors*.